FACTORS AFFECTING THE SHEAR STRENGTH OF COHESIONLESS SOIL

Thesis for the Degree of M. S.
MICHIGAN STATE UNIVERSITY

William Arthur Sack

1960

This is to certify that the

thesis entitled

Factors Affecting the Shear Strength
of Cohesionless Soil

presented by

William Arthur Sack

has been accepted towards fulfillment
of the requirements for

M.S. degree in Civil Engineering

Major professor

Date May 20, 1960

O-169

FACTORS AFFECTING THE SHEAR STRENGTH

OF COHESIONLESS SOIL

by

William Arthur Sack

AN ABSTRACT

Submitted to the College of Engineering
Michigan State University of Agriculture and
Applied Science in partial fulfillment of
the requirements for the degree of

MASTER OF SCIENCE

Department of Civil Engineering

1960

Approved: ~~~~~~~~~~~~~~

This thesis reports an investigation of the shear strength of a cohesionless soil by evaluating the frictional and volume change components of shear strength. The effects of initial void ratio, normal pressure, and particle shape on shearing resistance were also investigated.

Direct shear tests were made to determine the shear strength and the volume change of the soil during shear. Friction tests were performed on quartz to determine the variation of the coefficient of friction with normal pressure, W.

It was found that the shearing resistance increased almost linearly with increasing relative density. The increase was due primarily to the increase in the shear force necessary to do work against dilation.

The angle of shearing resistance, ϕ, decreases with increasing normal load by as much as 12°. The coefficient of friction for quartz as found from the shear tests and the friction tests decreases with increasing normal load in a manner similar to ϕ. It is believed that the decrease in ϕ with increasing W is due mainly to the frictional properties of the mineral.

The more angular sands have values of ϕ 2 or 3° higher than the round sand.

FACTORS AFFECTING THE SHEAR STRENGTH

OF COHESIONLESS SOIL

by

William Arthur Sack

A THESIS

Submitted to the College of Engineering
Michigan State University of Agriculture and
Applied Science in partial fulfillment of
the requirements for the degree of

MASTER OF SCIENCE

Department of Civil Engineering

1960

ACKNOWLEDGMENT

The author wishes to express his indebtedness and appreciation to Dr. T. H. Wu, Department of Civil Engineering, Michigan State University, whose generous help and encouragement made this thesis possible.

TABLE OF CONTENTS

LIST OF FIGURES

Figure		Page

LIST OF TABLES

SYMBOLS

A	area
B	a constant for a given material depending upon its stress-deformation behavior
D_R	relative density
d	diameter
E	modulus of elasticity
e	void ratio
e_o	initial void ratio
e_{max}	maximum attainable void ratio
e_{min}	minimum attainable void ratio
F	shear force
K	the ratio of shear strength to yield pressure for a given material $= \frac{S}{P_m}$
N	number of grains or spheres
p	load per particle
P_m	yield pressure of a metal
q_o	maximum pressure between two bodies in contact
R_1, R_2	radii of spherical grains
s	shear strength
W	normal load
w	work
Δm	the shearing displacement at which the maximum shearing resistance is obtained
$\delta(\Delta)$	displacement in the horizontal direction
$\delta(V)$	volume change per unit of area, (-) for compression, (+) for expansion

ϵ_1	unit strain in the direction of the major principal stress
ϵ_3	unit strain in the direction of the minor principal stress
θ	the angle whose tangent equals $\delta(v)/\delta(\Delta)$
μ	coefficient of friction
σ	normal stress
$\bar{\sigma}$	normal effective stress
$\sigma_1, \sigma_2, \sigma_3$	major, intermediate, and minor principal stresses
τ	shear stress
τ'	component of shear stress required to overcome the internal friction of the sample assuming the individual values of θ are equal to zero
τ''	the same as τ', but modified by the collapse of bridges (see dashed curve-figure 6).
τ_d	the additional shear stress required to produce failure because the plane of sliding is inclined at some angle to the shear stress (as computed by Newland and Allely's method)
τ_v	the shear stress required to do work against volume change (energy method)
τ_R	residual shear stress
ϕ	angle of shearing resistance
ϕ_c	the experimental values of ϕ corrected for variations in void ratio
ϕ_f	angle of internal friction corrected for volume change
ϕ_n	angle of internal friction as found by Newland and Allely's method
ϕ_R	the residual angle of shearing resistance
ϕ_μ	angle of sliding friction

I. FUNDAMENTAL CONSIDERATIONS

MOVEMENT OF SAND PARTICLES DURING SHEAR

The shear strength of a cohesionless material is dependent upon the type and magnitude of the inter-particle movements during shear as well as its frictional resistance. In 1925, Terzaghi (1)* pointed out that shear failure along a surface of sliding in sand occurs progressively and not suddenly. As the shearing stress increases, the resulting displacement increases more rapidly than the stress (incipient slip). This may be due to a rotational displacement of the sand particles without the particles changing their partners. The movement is resisted largely by the frictional resistance at the points of contact between grains. At constant shearing stress, the rate of increase of displacement decreases and eventually ceases. The particles on one side of the surface of sliding now begin to advance with reference to those on the other side. The length of movement is far more than a single particle diameter and hence the grains change partners. The resistance to this last displacement depends on the degree of interlocking of the grains and hence will increase with decreasing porosity. After a slip within the sand mass, the porosity of the sand adjacent to the interface is higher than that further away, and therefore the resistance to sliding will be smaller here than elsewhere in the mass.

*Numbers in parentheses indicate reference listed in Bibliography.

Mogami (2) found the movement of sand during shear to consist of two stages. He used a shear box having a light cover plate but did not apply a vertical load. In the first stage of the shearing motion, the sand layer near the shearing plane becomes loose and moves in a manner similar to a viscous liquid. The layer of motion has a finite breadth and the cover plate is heaved up continuously by the sand. In the second stage the motion of the sand becomes constant and is confined to a very thin layer. The heaving of the cover plate ceases and no vertical force is generated. The shearing force becomes constant.

Rowe (3) found that the angle of shearing resistance depends upon the degree of interlocking of the soil grains, which in turn depends upon the fractional movement of the shear planes, called slip strain. Slip strain does not increase in proportion to sample thickness. The decrease in sample thickness during shear is approximately proportional to the slip strain and is independent of thickness. This is in agreement with Mogami's observation that the sliding movement takes place within a narrow zone usually defined as the failure surface.

ANALYSIS OF SHEARING RESISTANCE BY ENERGY CONSIDERATIONS

Volume Change Correction

It is well known that a granular material undergoes a volume change during shear. Reynolds (4) was one of the first to study this relationship in 1886. He termed it dilatancy as the volume change is usually positive.

In 1948, Taylor (5) described the shear strength of sand as consisting of two parts. The first is the frictional resistance between grains, which is a combination of rolling and sliding friction. The second factor he called interlocking. The interlocking of the grains contributes a large part of the strength in dense sands. Taylor outlined a method for evaluating the effect of interlocking on shear strength in terms of strain energy.

Hafiz (6) also analyzed the volume change using energy considerations. Consider a sample of sand in a direct shear apparatus which is subjected to a normal effective stress $\bar{\sigma}$, and a shearing stress τ. A small displacement in the horizontal direction $\delta(\Delta)$ will then result in a positive volume change of $\delta(v)$ per unit area.

Work done by the applied shear stress is therefore $\tau\,\delta(\Delta)$ per unit area. The work is expended in causing the sample to dilate against normal effective stress $\bar{\sigma}$, and in overcoming the frictional resistance of the sample.

Denoting that part of the shear stress which is required to overcome the frictional resistance of the sample as τ'

$$\tau\delta(\Delta) = \tau'\delta(\Delta) + \bar{\sigma}\,\delta(v) \qquad \text{or}$$

$$\frac{\tau'}{\bar{\sigma}} = \frac{\tau}{\bar{\sigma}} - \frac{\delta(v)}{\delta(\Delta)} \tag{1}$$

ϕ_f will be called the angle of internal friction and represents that part of the shearing strength designated as τ'. ϕ_f is defined by

$$\tan\phi_f = \frac{\tau'}{\bar{\sigma}} \tag{2}$$

It should be noted here that the values of τ' and ϕ_f do not represent the actual mineral friction of the material. It is merely the value obtained after subtracting the force required to do work against dilation τv, from the total shear force. A further correction is necessary to obtain $\phi\mu$, the angle of sliding friction.

The angle ϕ, measured directly in the shear test, will be called the angle of shearing resistance and is equal to

$$\tan \phi = \frac{\tau}{\sigma} \tag{3}$$

<u>Relationship Between the Angle of Internal Friction, ϕ_f, and the Coefficient of Friction, μ</u>

(a) Direct Shear Test

Bishop (7) analyzed the relationship between ϕ_f and μ in terms of strain energy for the direct shear test. The analysis is made for the case of no volume change and takes into account the difference in magnitude of the three principal stresses at failure.

Consider a small element of a sample acted upon by the principal stresses σ_1 and σ_3 (figure 1a). The unit strain in the direction of σ_1 is ϵ_1 and in the direction of σ_3 is ϵ_3. Under constant volume conditions

$$\epsilon_1 = -\epsilon_3$$

For displacements in the sample equal to y and x

$$\tan \theta = y/x$$

$$\log \tan \theta = \log y - \log x$$

or $$\frac{1}{\tan \theta} (\sec^2 \theta \, d\theta) = \frac{dy}{y} - \frac{dx}{x}$$

$$= \epsilon_1 - (\epsilon_3) = 2\,\epsilon_1$$

and $$d\theta = 2\,\epsilon_1 (\sin \theta \cos \theta)$$

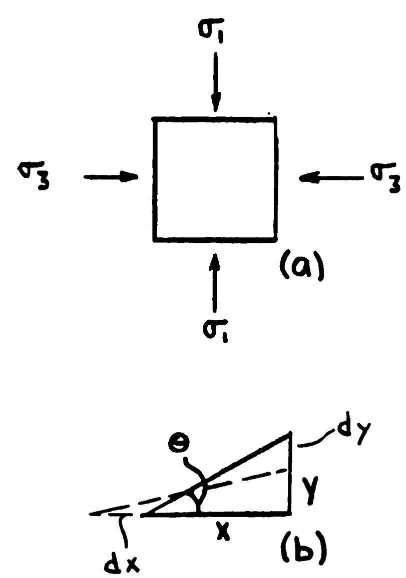

Figure 1

It is assumed that there will be an equal probability of contacts between grain surfaces in all directions. Considering a solid spherical element which has an equal projected area in all directions, the pairs of elements making up its surface will give the average work done per unit volume due to the combination of stress and strain in all directions.

If in a spherical element (see figure 2), a plane OA makes an angle θ with the σ_3 axis, the following relationships may be derived.

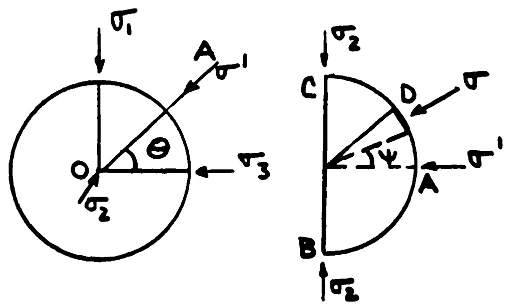

Figure 2

$$\sigma' = \sigma_1 \sin^2\theta + \sigma_3\cos^2\theta$$

For the plane including OA,

$$\sigma = \sigma_2 \sin^2\psi + (\sigma_1 \sin^2\theta + \sigma_3\cos^2\theta)\cos^2\psi$$

The force acting on an element at D is

$$(d/2)\ (d\psi)\ (d/2 \cos\psi)\ (d\theta)\ (\sigma)$$

Then displacement of the element is

$$\epsilon_1 \sin 2\theta\ d/2 \cos 2\psi$$

The work done against friction is

$$\epsilon_1 \sin 2\theta\ (d/2\cos\psi)\ (\mu)\ (\frac{d^2}{4}\cos\psi\, d\psi\, d\theta)$$
$$\left[\sigma_2 \sin^2\psi + (\sigma_1 \sin^2\theta + \sigma_3\cos^2\theta)\cos^2\psi\right]$$

Integrating around the slice BADC with respect to ψ from $-\pi/2$ to $\pi/2$, one obtains

$$\epsilon_1 \frac{\mu d^3}{8} \sin 2\theta\ d\theta \left[\sigma_2(\pi/8) + \sigma_1 \sin^2\theta + \sigma_3\cos^2\theta)\ (3\pi/8)\right]$$

Integrating around the sphere with respect to θ,

$$\text{Work} = w = \epsilon_1 \mu d^3\pi/32\ (3\sigma_1 + 3\sigma_3 + 2\sigma_2)$$

The energy per unit volume is

$$w\ \left(\frac{3 \times 8}{4 \times \pi \times d^3}\right)$$

$$\text{or}\quad \epsilon_1 \mu\ 3/16\ (3\sigma_1 + 3\sigma_3 + 2\sigma_2) \qquad (4)$$

Now at constant volume, the work done by σ_1 and σ_3 is

$$\frac{1}{2}(\sigma_1 - \sigma_3)\,\epsilon_1 \qquad (5)$$

By equating equations (4) and (5)

$$\sigma_1 - \sigma_3 = 3/8\ \mu\ (3\sigma_1 + 3\sigma_3 + 2\sigma_2) \qquad (6)$$

Assuming $\sigma_2 = a\ (\sigma_1 + \sigma_3)$ (7)

and substituting (7) into (6)

$$\frac{\sigma_1 - \sigma_3}{\sigma_1 + \sigma_3} = 3/8\ \mu\ (3 + 2a)$$

By Mohr's circle (figure 3)

$$\sin \phi_f = \frac{\sigma_1 - \sigma_3}{\sigma_1 + \sigma_3} = \frac{\sigma_1/\sigma_3 - 1}{\sigma_1/\sigma_3 + 1} \qquad (8)$$

Taking a = 1/2

$$\sin \phi_f = 3/8\ \mu\ (\ 3 + 1) = 3/2\ \mu \qquad (9)$$

(b) Triaxial Shear Test

The relation between ϕ_f and μ was analyzed for the case of the triaxial test using the same general approach.

In the case of the triaxial test, at constant volume

$$\epsilon_1 + \epsilon_2 + \epsilon_3 = 0 \text{ and } \epsilon_2 = \epsilon_3$$

$$\therefore\ \epsilon_3 = -\ \epsilon_1/2$$

For shearing strains in the body equal to y and x (see figure 1),

$$\tan \theta = y/x$$

and $d\ \theta = 3/4\ \epsilon_1 \sin 2\theta$

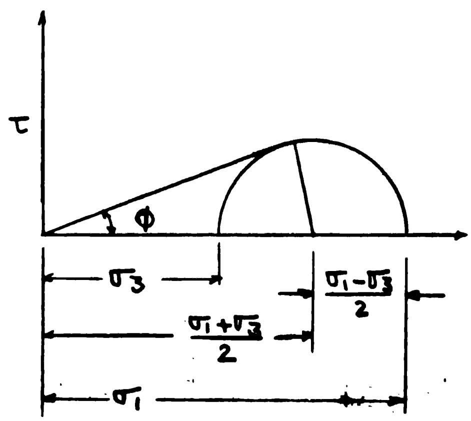

Figure 3

As in the case of plain strain, a solid spherical element will be used to compute the average work done per unit volume due to the combination of stress and strain in all directions. Then the force acting on an element at D (see figure 2) is

$$d/2 \times d\psi \times d/2 \cos\psi \times d\theta \times \sigma$$

A relative displacement of the element will be

$$3/4\ \ \epsilon_1 \sin 2\theta \times d/2$$

The work done against friction is

$$(3/4\ \epsilon_1 \sin 2\theta\ d/2) \times (\mu) \times (d^2/4 \cos\psi\, d\psi\, d\theta)$$
$$\times\left[\sigma_3 \sin^2\psi + (\sigma_1 \sin^2\theta + \sigma_3 \cos^2\theta)\cos^2\psi\right]$$

Integrating around the sphere with respect to ψ gives

$$3/32\ \epsilon_1 \mu\, d^3 \sin 2\theta\, d\theta\left[2/3\sigma_3 + (\sigma_1 \sin^2\theta + \sigma_3 \cos^2\theta)\,4/3\right]$$

Integrating with respect to θ yields

$$w = 4\int_0^{\pi/2} 3/32\ \epsilon_1 \mu\, d^3\ (2/3\sigma_3 \sin 2\theta + 8/3\sigma_1 \sin^3\theta\cos\theta$$
$$+ 8/3\sigma_3 \cos^3\theta \sin\theta)\, d\theta = 1/4\,\epsilon_1 \mu\, d^3\ (\sigma_1 + 2\sigma_3)$$

Hence energy per unit volume is

$$3/2\pi\ \epsilon_1 \mu\ (\sigma_1 + 2\sigma_3) \qquad (10)$$

Now at constant volume, the work done by σ_1 and σ_3 is

$$1/2\ (\sigma_1 \epsilon_1 + 2\sigma_3 \epsilon_3) \qquad \text{and since } \epsilon_3 = -\epsilon_1/2$$

$$w = \frac{\epsilon_1}{2}(\sigma_1 - \sigma_3) \qquad (11)$$

By equating equations (10) and (11)

$$\frac{3}{2\pi}\epsilon_1 \mu\ (\sigma_1 + 2\sigma_3) = \frac{\epsilon_1}{2}(\sigma_1 - \sigma_3)$$

$$\text{and } \frac{\sigma_1}{\sigma_3} = \frac{\frac{3}{\pi}\mu + 1}{\frac{3}{2\pi}\mu - 1}$$

Then from equation 8

$$\sin\phi_f = \frac{9\mu}{3\mu + 2\pi} \qquad (12)$$

ANALYSIS OF SHEARING RESISTANCE BY CONSIDERATION OF INTER-PARTICLE MOVEMENTS

Newland and Allely (8) analyzed inter-particle movement to explain the effect of dilatancy on shear strength. Figure 4 shows a shear stress applied in a horizontal direction, causing particles a, b, c, etc., to move to the right relative to particles a', b', c', etc. Excluding grain failure, for particle a to move to the right relative to particle a', it must initially slide in a direction making an angle θa to the direction of the shear stress. Each particle, therefore, has a component of movement in the vertical direction and the mass consequently expands against the normal stress.

Forces parallel and perpendicular to the initial direction of movement of particle a may be resolved as

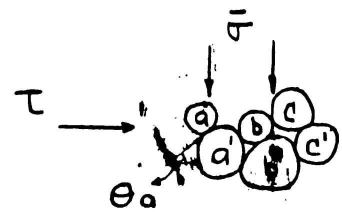

Figure 4

$$\frac{\tau a \; Aa \cos \theta a - \bar{\sigma} \; Aa \sin \theta a}{\tau a \; Aa \sin \theta a + \bar{\sigma} \; Aa \cos \theta a} = \tan \phi_\mu$$

Here ϕ_μ is defined as the angle of sliding friction and $\tan \phi_\mu$ is the coefficient of friction. Simplifying,

$$\tau a \; Aa = \bar{\sigma} \; Aa \; (\tan \phi_\mu + \theta a)$$

Similar relationships may be obtained for other surfaces of sliding as

$$\frac{\tau}{\bar{\sigma}} = \frac{Aa \tan (\phi_\mu + \theta a) + \ldots A_n \tan (\phi_\mu + \theta_n)}{A_a + A_b + \ldots\ldots\ldots\ldots A_n} \qquad (13)$$

Now if particle a moves a distance $\delta(\Delta)$ in the direction of the shear stress, it raises against the normal stress $\bar{\sigma}$ a distance $\delta(\gamma a)$ such that

$$\tan \theta = \frac{\delta(\gamma a)}{\delta(\Delta)}$$

Then considering the mass as a whole,

$$\tan \theta = \frac{\delta(v)}{\delta(\Delta)} \qquad (14)$$

As sliding begins, the individual values of θ are a maximum except in very loose sands. Hence the shear stress and rate of volume expansion will attain maximum values of τmax and $\frac{\delta(v)}{\delta(\Delta)}$max. τmax may be considered to consist of a shear stress τ' necessary to overcome the frictional force, assuming the individual values of θ are equal to zero ($\tau' = \tan \phi_\mu$), plus the shear stress τ_d required to overcome the resistance to expansion against $\bar{\sigma}$ because the individual planes of sliding are inclined at some angle to the shear stress.

As the shear displacement proceeds, the shear stress drops to a residual value, τ_R. If at that point the expansion $\frac{\delta(v)}{\delta(\Delta)}$ has ceased, then the average value of θ is equal to zero. Then τ_R should equal the computed value of τ'. The residual angle of shearing resistance ϕ_R is then equal to ϕ_μ.

Equations (13) and (14) have not taken into account the fact that the movement of each particle will be restricted by the movement of its neighboring particles. Conceivably, the particles having the steepest initial surface of sliding may control the expansion with the remaining particles "bridging" over their former contacts as shown in Figure 5. Due to the normal load, the bridges may continually develop and collapse as shown in Figure 6.

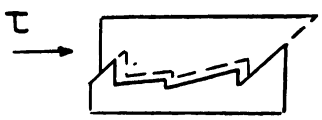

Figure 5

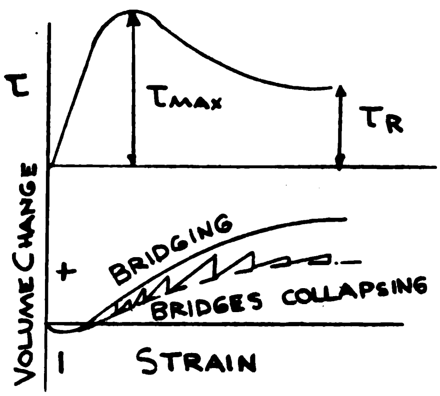

Figure 6

The slope of the steep-rising portion of the stepped curve in Figure 6 is that which should be used with the peak value of the shear stress in equation 13 to obtain the true value of ϕ_u. If the flatter slope of the experimental dashed curve is used, the value of ϕ_u obtained will be larger than the true value. Because of the continuous collapse of the bridges, a measured $\frac{\delta(v)}{\delta(\Delta)}$ of zero does not always mean that θ is zero. Hence, the computed

ϕ_μ and τ' are dependent upon the mode of failure as well as the coefficient of friction and will be called ϕn and τ''. ϕn is called the angle of internal friction. Equation 13 now becomes

$$\frac{\tau_{max}}{\sigma} = \tan(\phi n + \theta max) \tag{15}$$

and

$$\theta max = \tan^{-1} \frac{\delta(V)max}{\delta(\Delta)} \tag{16}$$

Then

$$\phi n = \tan^{-1} \frac{\tau''}{\sigma} = \phi - \theta \tag{17}$$

The shear stress represented by θ is called τ_d.

Hence by Newland and Allely's analysis, θ is deducted from ϕ to obtain ϕn. The value of ϕn so obtained will be equal to ϕ_μ only if complete "bridging" occurs.

The value of ϕn found from equation 17 will be equal to the residual shear strength ϕ_R, when $\frac{\delta(V)}{\delta(\Delta)} = 0$, only if the mode of failure at the end of the test is the same as it is at the peak point. Since it has been mentioned that because of the collapse of bridges the measured $\frac{\delta(V)}{\delta(\Delta)}$ is not a reliable indication of θ, it is not likely that ϕn will be equal to ϕ_μ or ϕ_R.

II. FRICTION

NATURE OF FRICTION

The experimental laws governing friction state that frictional resistance is directly proportional to the load and is independent of the size of the surface in contact.

Metals

Much more is known about the frictional behavior of metals than of non-metals. F. P. Bowden (9), who is well known for his studies of frictional resistance, explains the laws of friction in terms of the surface contour of solid surfaces. The engineers best surfaces have irregularities which are thousands of angstrom units high (Figure 7). Electrical conductivity experiments have found that for flat steel surfaces, the actual area of contact may be only one ten-thousandth of the apparent area. Thus the actual area of contact depends mainly on the load which is applied to the surfaces and is directly proportional to it. Therefore, even with lightly loaded surfaces, the local pressure at these small points of contact is very high and may cause the hardest metals to flow plastically until their cross sectional area is sufficient to support the applied load. The two surfaces thus adhere or weld

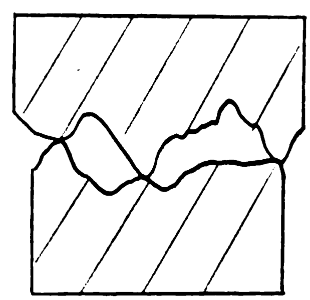

Figure 7

together at points of contact. The actual area of contact is

$$A = W/P_m \tag{18}$$

where W is the load and P_m is the yield pressure of the metal.

Bowden[9] states that there is strong evidence that the friction of metals is due, in large measure to adhesion at these contact regions and represents the force necessary to shear these junctions. The friction, F, is approximately equal to As, where s is the shear strength of the junctions. For most solids, whether plastic, brittle, or elastic, the surface adhesion can be strong.

Since the real area of contact is directly proportional to the load, so is the friction. The value of the coefficient of friction μ, will then be a constant since

$$\mu = \frac{F}{W} = \frac{As}{W} = \frac{W}{P_m} \times \frac{S}{W} = K \tag{19}$$

The characteristic frictional properties of metals are seen to be due largely to their ability to flow plastically and to weld together under load.

Non-Metals

Some non-metals have frictional characteristics similar to metals while others are quite different. Extensive studies were made by Bowden and Young (10) to investigate the frictional behavior of diamond. The deformation of diamond was found to be principally elastic rather than plastic and hence the real area of contact is expected to be proportional to $W^{2/3}$ rather than W. The coefficient would no longer have a constant value, but vary as $W^{-1/3}$ since

$$\mu = \frac{F}{W} = \frac{As}{W} = \frac{W^{2/3}s}{WP_m} = KW^{-1/3} \tag{20}$$

Experimentally, μ varies as $KW^{-0.2}$ for clean degassed diamond surfaces. This indicates that the deformation is largely elastic.

The adsorbed surface film of oxygen and other gases normally present has a marked effect on friction. For clean diamond exposed to air, μ is about. 085 at a load of 10 grams. With the adsorbed gases removed and specimen tested in vacuo, μ increases to almost .45.

The orientation of the crystallographic axis of the mineral to sliding has a large effect upon its resistance to sliding.

FRICTION EXPERIMENTS ON MINERALS

Hafiz investigated the frictional characteristics of quartz and flint. A block of a mineral was cut flat and its face roughened. Three 1/8 inch diameter particles were then slid over the block under various normal loads. For both minerals, the value of ~~ϕ~~ μ decreases with increasing loads as shown in Figure 8. The average sliding value is given in Figure 8. The value of μ for quartz ranges from .380 to .492, and for flint .274 to .366 depending on the normal load.

Tschebotarioff and Welch (11) conducted a series of friction tests on quartz, calcite, pagodite, and pyrophyllite under dry, moist, and completely submerged conditions. Dry tests were performed immediately after removing the minerals from the desicator. A two inch polished cube of each mineral was slid over mineral fragments at normal loads up to about 36 lb.

The value of the friction remained almost constant for all loads. The value of μ for quartz varied from .11 in the dry condition to .45 when submerged and the corresponding values of μ for calcite were .11 and .26.

A distinct difference exists between the frictional characteristics of the hydrophilic minerals, quartz and calcite, which have an affinity for water; and the hydrophobic minerals of the talc variety which are water repellent. Water has a slight lubricating effect on the hydrophobic minerals and decreases the frictional resistance. However, water significantly increases the frictional coefficient for the hydrophilic minerals.

Penman (12) investigated the coefficient of friction for quartz. Two fairly large quartz crystals were imbedded in plaster and tested at a constant rate of strain. The surfaces were washed with soap and water, rinsed with distilled water and submerged during testing. The measured frictional coefficient is .650 for normal loads ranging from 2.96 lbs. to 151.3 lbs. For quartz crystals dried in an oven at 105° C and tested while warm, the value of is .195 for the same range of normal loads. The area of the upper quartz surface is about 1.2 sq. inches so that the maximum test load is about 126 psi. No damage on the quartz surfaces was reported.

To produce higher stresses, three freshly broken chips were moved over the lower quartz surface while saturated with distilled water. For normal loads increasing from 4.1 to 145 lbs., μ decreases from .555 to .345. Crushing of the points was noted at all loads above 100 lbs. The coefficient of friction thus decreased from .650 for a normal load of 126 psi to .345 at a much higher load.

Recently (1959), friction tests were carried out at the Norwegian Geotechnical Institute (13). Three points of a mineral were slid over a crystal at a constant velocity while submerged under various liquids. The value of μ for quartz varies from about .0625 to .141 when submerged in water, and from .156 to .312 when submerged in alcohol. The load varied from about 5 to 35 gms per point. Both the load and the direction of sliding influence the coefficient. The value of μ decreases with increasing normal load for some directions of sliding, while in others, it is constant.

Shear Strength of a Loose Sand. A series of triaxial tests at the Norwegian Geotechnical Institute (NGI) (14) on a fine loose sand (primarily composed of quartz) produced some unexpected results. Using the consolidated undrained constant volume test, at initial porosities near 43 per cent the angle of internal friction is about 35°. However as the porosity increases from 43 to 47.5 per cent, ϕ_f drops off sharply to around 12°. High pore pressures were recorded in the tests on the very loose sands.

It seems probable that the very low values of ϕ_f obtained represent mainly the frictional resistance of the mineral grains (i. e. $\phi_f \sim \phi\mu$). If so, this is in agreement with the results of friction tests at NGI. Assuming that the value of $\phi\mu$ is equal to 12° (μ = .213), the value of ϕ_f computed from equation 12 is 16.1°, which is rather low. In other words a value of μ equal to 12° cannot account for an angle of internal friction of 35°.

SUMMARY

From the work of Bowden and Tabor, it is seen that friction between two surfaces will depend on the true area of surface contact.

For materials that behave plastically, the actual area of contact increases in direct proportion to the load and hence μ is constant. However, for non-plastic materials, the true area does not increase in direct proportion to the load and μ is not a constant. For an elastic material, μ is proportional to the -1/3 power of W.

Large differences in the value of μ for the same mineral have been reported in the literature. Penman, Tschebotarioff, and Hafiz found the value of μ for quartz to range from .345 to .650 when moist or submerged in water and from .11 to .195 when dry. The lower values were obtained at high normal stresses. However the friction tests at NGI (under submerged conditions) resulted in values of μ from .0625 to .141, while triaxial tests gave values of ϕ_μ as low as 12° ($\mu = .213$). The values of μ obtained at NGI seem quite low when compared with the other tests.

III. EXPERIMENTAL PROGRAM

OBJECT

The purpose of the experimental program is to examine the shear strength of a cohesionless soil by an evaluation of the frictional and dilatancy components. It is believed that a study of these components and the factors influencing their relative magnitude would improve the understanding of shearing resistance, and facilitate in prediction of the behavior of a soil under various load conditions in the field. The investigation includes the effects of initial voil ratio, particle shape, and normal pressure.

PROPERTIES OF THE SANDS INVESTIGATED

Angularity

Three sands with very different particle shapes were used in the tests. Ottawa sand was used because of its characteristic roundness. A typical Michigan glacial sand was used as a sub-angular soil, and a residual sand from Georgia containing specs of mica was tested because of its extremely angular grains. Micrographs of the angular sands are shown in Figures 9 and 10.

The roundness and sphericity of the sub-angular and very-angular sands are 0.390, 0.800; and 0.175, 0.787 respectively. Roundness is defined by Wadell (15) as $\Sigma\frac{r}{R}/H$ and sphericity as d_c/D_c where

H = number of corners on a grain

R = the radius of the maximum inscribed circle

r = the radius of curvature of a corner

d_c = diameter of a circle equal in area to the area obtained when the grain rests on one of its larger faces

D_c = diameter of the smallest circle circumscribing the grain reproduction

Minerals

The ottawa sand is composed of quartz, while the angular sand contains a mixture of feldspar, quartz, and other minerals usually found in glacial soils. The very-angular sand contains a significant amount of mica.

Grain Size-Graduation

Two different ranges in particle size were tested.

Sand type A contains only grain sizes from .590 to .297 mm in diameter. This is the size range that passes a #30 U.S. standard sieve and is retained on a #50 sieve.

Sand type B contains grain sizes from .250 to .149 mm in diameter. These grain sizes pass a #60 U.S. standard sieve and are retained on a #100.

The majority of the experimental work was performed using sand type A. Hence the following discussion refers to type A unless otherwise specified.

Maximum and Minimum Void Ratio

In order to compute relative density D_R, the sands were tested to find their respective maximum and minimum void ratios. Methods developed by J. J. Kolbuszewski (16) were used. To obtain the loosest possible state (highest void ratio), 250 grams of dry sand were placed in a one liter graduated cylinder. The cylinder was shaken a few times, turned upside down, and then very quickly turned over again. The volume of the sample was read and its void ratio calculated.

The densest state was obtained by using a vibrating table. The sand was placed in a brass mold, 3 inches in diameter and 3 inches deep, which was clamped to the table. A tight fitting cap was placed on the sand and a 100 gram weight was placed on top of the cap. The sand was placed in 3 layers and vibrated 5 minutes for each layer. The void ratios obtained are shown in TABLE I.

SHEAR TESTS

Dry Triaxial Tests

A series of dry triaxial tests were performed at various degrees of compaction. The specimens were approximately 1.45 inches in diameter and 3.10 inches long. A schematic diagram of the triaxial apparatus is shown in Figure 11.

A constant all around effective stress $\bar{\sigma}_3$, of about .960 Kg/cm^2 was used in all tests. A vacuum was applied to the sample through the burette B (Figure 11), thus utilizing atmospheric pressure to supply $\bar{\sigma}_3$.

The deviator stress was applied at a rate of approximately 0.4 per cent per minute until failure.

Consolidated Undrained Triaxial Tests

A series of consolidated undrained (CU) triaxial tests were carried out in an attempt to study the effect of an extremely high void ratio. To obtain the highest possible initial void ratio, the sand was carefully placed in the membrane at a moisture content of about 11 per cent. At this moisture content the capillary forces create an adhesion between the grains resulting in a "honeycombe" structure. The sample was then saturated at either a very fast or a very slow rate in an attempt to allow only a minimum of consolidation as the capillary tensions were destroyed. The time allowed to saturate the sample varied from one to as much as 90 minutes.

The sample was then subjected to a very light vacuum of 1 to 3 inches of mercury through the burette (B in Figure 11), the mold removed and the dimensions of the sample measured. Specimen sizes were the same as those used in the dry triaxial tests above.

After consolidation by a hydrostatic pressure σ_3, the cell pressure was increased and at the same time a porewater pressure of the same magnitude was applied. This procedure was followed in an attempt to completely saturate the sample by compressing and dissolving the air bubbles in the porewater. As the cell pressure and pore pressure were increased simultaneously, the effective stress remains unchanged. Pore pressure measurements were made by balancing the water level in the capillary tube A as shown in Figure 11.

The specimen was then sheared at a constant σ_3 under constant volume conditions by the application of a deviator stress.

Direct Shear Tests

Well over 50 direct shear tests were made under both saturated and dry conditions. The direct shear apparatus used takes a circular specimen 2.5 inches in diameter and approximately 0.8 inches high. The shear stress τ, was applied at a rate of approximately 1.0 per cent per minute.

Sand types A and B were tested with the majority of tests run on type A.

<u>Friction Tests</u>

Friction tests were run on quartz crystals to check the variation in the coefficient of friction with normal load. The direct shear apparatus was adapted for this purpose. A quartz crystal approximately $1\frac{1}{4}$ inches long and $\frac{1}{4}$ inch wide was set into a block of plaster of paris which was carefully sized to fit into the stationary part of the shear apparatus. Another crystal was set in a similar manner into the movable (top) half of the shear apparatus so that its point would bear on the stationary crystal (see Figure 12).

The quartz was not polished or cleaned in any manner so as to leave its surface in the same condition as that of the sands tested.

Both dry and saturated tests were made with normal loads from 1 to 24 Kg.

IV. RESULTS OF TESTS

SHEAR STRENGTH FROM DIRECT SHEAR TESTS

The results of the direct shear tests are summarized in TABLES II, III, and IV. The shear strength was divided into frictional and volume change components by the energy method and by Newland and Allely's particle movement method. The angle of internal friction ϕ_f, as found by the energy method, was calculated using equations 1 and 2. The angle of internal friction by Newland and Allely's method, ϕn, was computed by equations 15, 16, and 17. The calculated ϕ_f and ϕn are also given in TABLES II, III, and IV.

The value of ϕ varies from 43.9° to 29.3°, while the computed value of ϕ_f ranges from 41.8 to 26.5°. Newland and Allely's analysis yields values of ϕn from 40.1° to 25.7°.

Typical stress-strain curves are shown in Figures 13, 14, and 15 for the 3 sands. Values of tan ϕ, tan ϕ_f and the maximum value of ϕn are plotted versus the horizontal displacement. The volume change is shown below the stress-strain curves in each case.

The ultimate or residual shear strength of the sands is taken at the part of the stress-strain curve where the volume change has ceased such as point "a" in Figures 13, 14, and 15.

Effect of the Initial Void Ratio

The increase in the angle of shearing resistance ϕ, with decreasing void ratio is a well known relation. The greater shear strength exhibited by a dense material is due mainly to interlocking of the particles. It would be expected then, that the shear force required to cause dilation, τ_v, would account for most of this increase in strength and that ϕ_f would be almost unaffected by density.

Figures 16, 17, and 18 show the results of the direct shear tests. Values of ϕ, ϕ_f, ϕn, and ϕ_R are plotted against e_o for a normal stress of .7575 Kg/cm^2. The value of ϕ is seen to vary as much as 8^o. However, ϕ_f and ϕ_R remain nearly constant for all values of e_o thus confirming the concept that τ_v is mainly responsible for the variation of ϕ with e_o. However, ϕn increases significantly with increasing e_o.

The value of τ_v and τ_d expressed as the per cent of the total shearing resistance increases with decreasing e_o as shown in TABLES II, III, and IV. The average values of τ_v and τ_d are 16.9 per cent and 23.7 per cent respectively for the 3 sands.

Effect of Relative Density

The relative density of a soil is defined as

$$D_R = \frac{e_{max} - e}{e_{max} - e_{min}} \tag{21}$$

Hence, a soil in its densest possible state would have a D_R of 100 per cent and in its loosest possible state a D_R of 0 per cent.

The values of ϕ, ϕ_f, ϕn, and ϕ_R are plotted against D_R in Figure 19 for the sub-angular sand. It may be seen that ϕ increases almost linearly with increasing D_R as would be expected. ϕ_f and ϕ_R however, which have very similar values, are almost independent of D_R. The value of ϕn decreases with increasing D_R.

To study the effect of D_R on the shear strength due to volume change, the percentages of τ_v and τ_d are related to D_R in Figures 20 and 21. The values of τ_v and τ_d as a percentage of the total shear strength increase with increasing D_R. It is interesting to note that the curves for the 3 sands are quite similar.

Effect of Normal Load

Taylor and others have reported that ϕ is also dependent on normal pressure. A series of tests were performed varying the normal load from 8 to 32 Kg. An attempt was made to keep the variation in e_o to a minimum.

The angle of shearing resistance decreases up to 10.6^o with increasing load as is shown in Figures 22, 23, and 24. The angles of internal friction, ϕ_f and ϕn, decrease with increasing W by an amount similar to ϕ. This indicates that the components of shear strength attributed to τ_v and τ_d (which had already been deducted from ϕ to obtain ϕ_f and ϕn respectively) are not responsible for the decrease. The decrease is believed to be primarily a function of the frictional characteristics of the mineral grains as discussed in a subsequent part of this paper.

In order to compensate for changes in ϕ which may have been due to variations in e_o, the relationships between ϕ and e_o (Figures 16, 17, and 18) were used to correct the experimental values. The corrected ϕ versus e_o curves are also plotted in Figures 22, 23, and 24 and are designated as ϕ_c.

Effect of Particle Shape

A sand containing angular grains is expected to have a higher shear strength than a sand with predominantly round grains. Figure 25 shows the results of the direct shear tests on the round (ottawa), sub-angular (glacial), and very-angular (residual) sands. The values of ϕ, ϕ_f and ϕn are plotted against D_R for each sand.

There is no significant difference in the shearing resistance of the sub-angular and very-angular sands. However, the round sand is seen to have values of ϕ, ϕ_f, and ϕn which are 2 to 3 degrees lower than the other sands. One reason for this difference may be that it requires more work to roll and slide a random arrangement of cubes over one another than spheres.

It must be recognized here that the difference between the shearing resistance of the round and angular sands shown in Figure 25 is also influenced by the mineral composition of the sands.

Strain at Maximum Shear

To obtain a better insight into the various factors contributing to the volume change component of shear strength, an analysis was made of the shear displacement at which the maximum shear occurred, Δm.

The tests indicate that Δm (see TABLES II, III, and IV) is influenced mainly by 3 factors. These factors are initial void ratio, grain shape, and particle size. A low initial void ratio causes the maximum shear resistance to occur at a lower strain than a high initial void ratio. The maximum shear occurs at a smaller strain for the round than for the angular sands. The value of Δm is smaller for type B sand (which contained smaller grains) than for type A sand.

At maximum shear strength all sands show expansion even though they had at first contracted. The particle diameter of the sand ranges from 0232 to .00586 inches while the strain at maximum shear ranges from .035 to .150 inches.

The observed relationship between Δm and e_o may be explained as follows. When a normal load is applied to a very loose sand the whole mass undergoes consolidation. As the sand is subjected to a shearing strain (as in the direct shear test) the particles in and around a relatively narrow shearing zone will consolidate without changing partners until they attain a certain critical density or void ratio. At this point the grains in the shear zone begin to rise up on one another causing expansion of the mass against W. This results in a maximum value of the shear stress. In a very dense sand however, as shearing takes place there is little or no consolidation of the particles in the shearing zone. Therefore at a relatively small strain the particles begin to slide and roll over one another producing a maximum value of τ.

As noted above, the round sand reaches its maximum shear strength at a lower strain than the more angular sands. A possible explanation for this might be that the round sand consolidates more readily during shear and hence reaches its critical density very quickly. Expansion thus begins at a lower strain.

It was found that Δm is smaller for sands with smaller grains. Since maximum shearing resistance occurs as the particles rise upon one another expanding against W, it would be expected that expansion would begin sooner in a finer sand, thus causing Δm to occur at a relatively low strain.

DRY TRIAXIAL TESTS

A series of dry triaxial tests were performed for comparison with the direct shear tests. Pertinent data from the tests are shown in TABLE V. The effective normal stress on the shear plane $\bar{\sigma}$, was maintained at about 1.52 Kg/cm^2 for all tests. The values of ϕ obtained are plotted against e_o in Figures 26, 27, and 28 (line B).

Line A in Figures 26, 27, and 28 represents the results of direct shear tests at a $\bar{\sigma}$ of .7575 Kg/cm^2. Using equation 23 (see page 28), and the respective values of K and B as found for each sand, the values of ϕ were corrected to a normal pressure of 1.52 Kg/cm^2 to obtain a better comparison with the triaxial tests. The computed values are shown as line C.

The values of ϕ as obtained from the direct and triaxial tests are seen to agree within 1 or 2^o except for the sub-angular sand where there is a 4^o difference. The agreement is believed to be good considering the limited number of triaxial tests performed.

It has been suggested by Hill[17] that in the direct shear test, the deformation is so constrained as to be effectively a simple shear in a narrow zone. The direct shear tests thus give a Mohr stress envelope such as a in Figure 29. The triaxial test, however, gives a tangent to the stress circle such as b. Thus the relation between the shearing resistance as obtained by the triaxial and the direct shear test would be

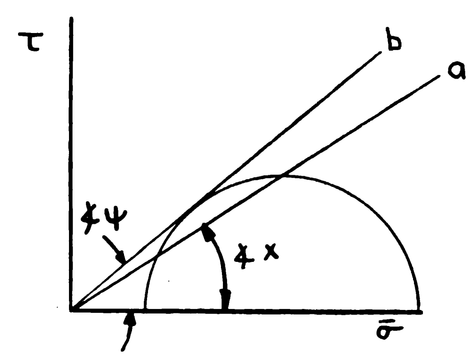

Figure 29

$$\sin\psi = \tan x \qquad (22)$$

The values of ϕ from the triaxial tests were reduced by equation 22 in order to give a comparison with envelope a. The values obtained are plotted as line D in Figures 26, 27, and 28. The agreement between the two is not satisfactory.

CONSOLIDATED UNDRAINED TRIAXIAL TESTS

Figure 30 shows a typical plot of deviator stress and pore pressure versus per cent strain for a typical test. The porosity is 41 per cent and the value of ϕ_f is 32.8^{o}. Since the tests are not successful in producing extremely high porosities with exceptionally low values of ϕ_f, the series was discontinued.

RELATIONSHIP BETWEEN SHEAR STRENGTH AND FRICTION

Friction Tests

The results of the friction tests on quartz are shown in Figure 31. It may be seen that the coefficient of friction is not a constant, but is a function of W. The data was found to follow the general equation

$$\mu = KW^{-B} \qquad (23)$$

K and B are constants depending upon the stress-deformation characteristics of the material.

The values of K and B are equal to 0.629 and 0.138. No significant change in μ was observed when the quartz surfaces were saturated with water. When the normal load exceeded 16 Kg., pieces of the point broke off and the lower quartz surface was damaged.

Friction From Direct Shear Tests

The coefficient of friction was computed for each direct shear test using equation 9. The computed coefficients for the 3 sands decrease with W according to equation 23. For the round, sub-angular, and very-angular sands the respective values of K and B are 0.491, 0.139; 0.489, 0.0965; and 0.610, 0.171. These values fall in the same range as the values obtained from the friction test.

The angle of sliding friction ϕ_{μ} is plotted against W in Figures 32, 33, and 34. The values of ϕ_c, ϕ_f, ϕn, and ϕ_R are shown for comparison.

It may be seen that the decrease in ϕ_R, ϕ, ϕ_f, and ϕn, with increasing W is similar to that of ϕ_{μ}. Hence it seems that the decrease in shearing resistance with increasing normal load is primarily a function of the frictional properties of the minerals involved.

(a) Comparison of Normal Stresses During Shear

In order to better compare the values of μ measured in the friction tests with those calculated from the shear tests, it is necessary to estimate the contact stresses between the sand particles in the shear tests.

Assuming the particles are spherical, Hafiz computed the contact load per particle for extremely loose and dense configurations. For particles in a loose rectangular pattern (Figure 35), each sphere touches six others. Then in a cross section of area A, the number of spheres is N, the diameter of each sphere is d, and

$$N = A/d^2$$

For a normal load of W, the load per particle, p, will be

$$p = \frac{Wd^2}{A}$$

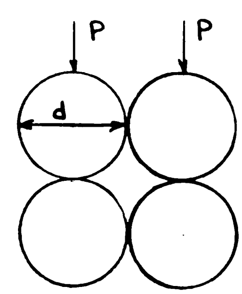

Figure 35

In a dense rhombic type packing, each particle touches twelve others. It may be seen from Figure 36 that

$B = 45^o$, $\psi = 45^o$ and $W/n = 4\ p \cos\psi = \frac{4p}{\sqrt{2}}$

then $p = \frac{W}{2.83N} = \frac{Wd^2}{2.83A}$

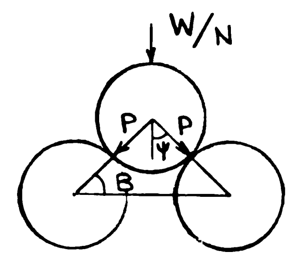

Figure 36

The loose packing has a void ratio of 0.92 and the dense 0.35.

Assuming that the average void ratio of the sands is midway between the dense and loose packs, the load per particle p would be

$$p = \frac{.677Wd^2}{A} \tag{24}$$

Using equation 24, the approximate load per particle was computed for each normal load and is shown in TABLE VI.

The contact pressure between particles was computed with the Hertz Equations (18) for an elastic material. For two spherical bodies in contact, the maximum pressure, q_o, is

$$q_o = 0.388 \sqrt[3]{WE^2 \frac{(R_1 + R_2)^2}{R_1^2 + R_2^2}} \tag{25}$$

and in the case of a ball pressed into a plane surface,

$$q_o = 0.388 \sqrt[3]{\frac{WE^2}{R_2^2}} \tag{26}$$

In these equations,

W = Normal Load

E = Modulus of Elasticity

R_1, R_2 = radius

An average modulus for quartz may be taken as 9.25×10^8 gms/cm^2 (19).

The radius of the quartz point was estimated to be between 1/16 inch and 1/8 inch. The coefficient of friction is plotted against q_o for the direct shear tests and the friction tests in Figure 37. The contact pressure computed from Hafiz's friction tests is also plotted in Figure 37.

The curve for friction tests is not in agreement with those for the direct shear and the friction tests by Hafiz. At least part of the difficulty lies in the uncertainty of the radius of the quartz point.

V. CONCLUSION

VOID RATIO AND RELATIVE DENSITY

The well known increase in shearing resistance with decreasing e_o or increasing D_R is primarily due to the increased shear force necessary to cause dilation against W. The angle of shearing resistance as well as the part of the shear strength necessary to overcome volume change increase almost linearly with increasing D_R.

ϕ_f and ϕ_R, which were found to be quite similar, are essentially independent of e_o and D_R. The value of ϕn, however, increases with increasing void ratio.

NORMAL LOAD

The angle of shearing resistance was found to decrease as much as 12^o with increasing normal load, W. The values of ϕ_f and ϕn decrease with increasing normal load by an amount similar to ϕ. Since the dilatancy components have already been deducted from ϕ to obtain ϕ_f and ϕn, the decrease in shearing resistance with increasing W cannot be due to dilatancy.

PARTICLE SHAPE

The values τ_v and τ_d as a percentage of the total shear strength for the 3 sands are quite similar when plotted against D_R. The more angular sands have values of ϕ, ϕ_f, ϕn, and ϕ_R 2 or 3^o higher than the round sand.

COMPARISON OF THE ENERGY AND PARTICLE DISPLACEMENT METHODS OF ANALYSIS

The analysis of the shear strength by the energy method leading to ϕ_f and ϕ_μ seems to yield quite consistent results. However, the analysis of particle displacements gives values of ϕn which increase with the initial void ratio. The uncertainties concerning the mode of failure make the physical significance of ϕn rather dubious.

FRICTION

The coefficient of friction was found to be a function of W in both the friction and the direct shear tests. The data was found to fit the general equation

$$\mu = KW^{-B}$$

The values of K and B for the friction tests are 0.629 and 0.138. In the direct shear tests, the respective values of K and B for the round, sub-angular, and very-angular sands are 0.491, 0.139; 0.489, 0.0965; and 0.610, 0.171.

As W increases, ϕ_μ decreases in a manner similar to the decrease in ϕ_R and ϕ. It is therefore believed that the decrease in shearing resistance with increasing normal load is mainly due to the frictional properties of the mineral.

The frictional resistance between two minerals will increase as the true area of contact between them. For both the friction test and the direct shear test on the quartz sand, the value of B was approximately 0.139. The true area of contact A is proportional to $W^{0.861}$. Hence, the deformation behavior of the quartz lies between the elastic (A proportional to $W^{2/3}$) and the plastic (A proportional to W) states.

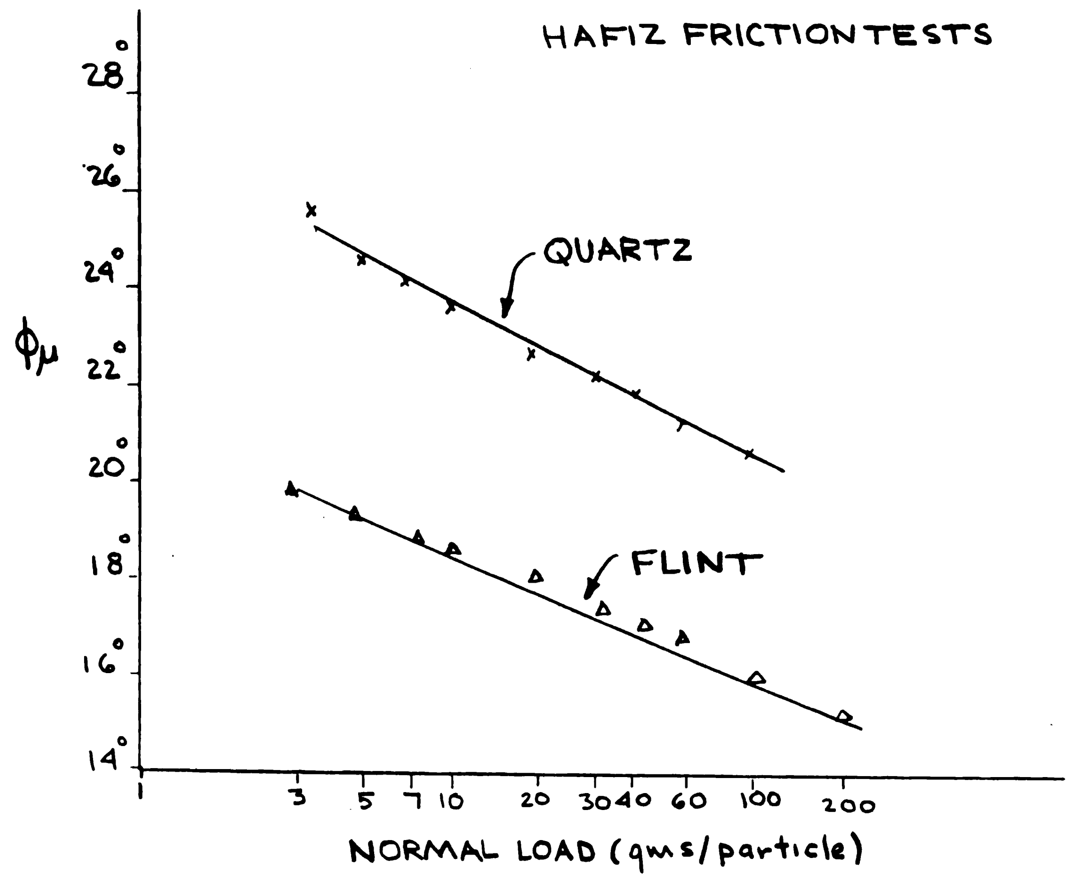

FIGURE 8

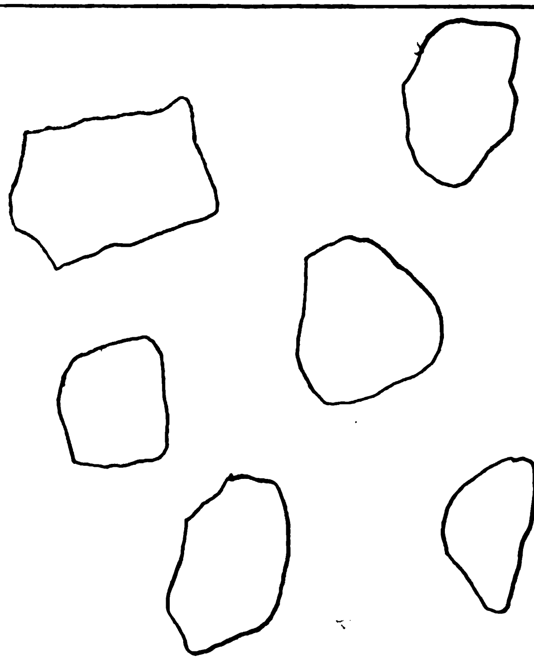

SUB-ANGULAR SAND

FIGURE 9

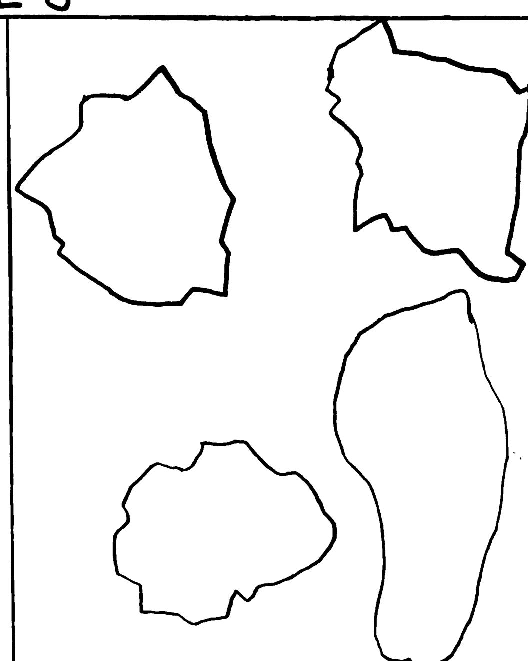

VERY-ANGULAR SAND

FIGURE 10

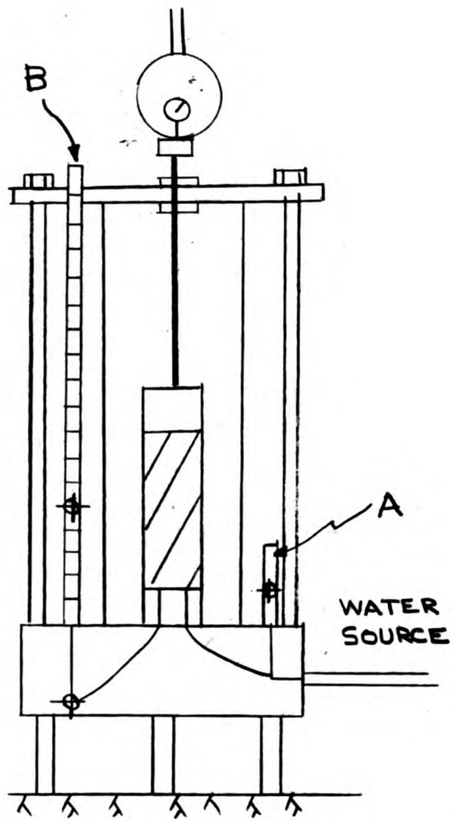

SCHEMATIC DIAG. TRIAXIAL CELL

FIGURE 11

FRICTION APARATUS

FIGURE 12

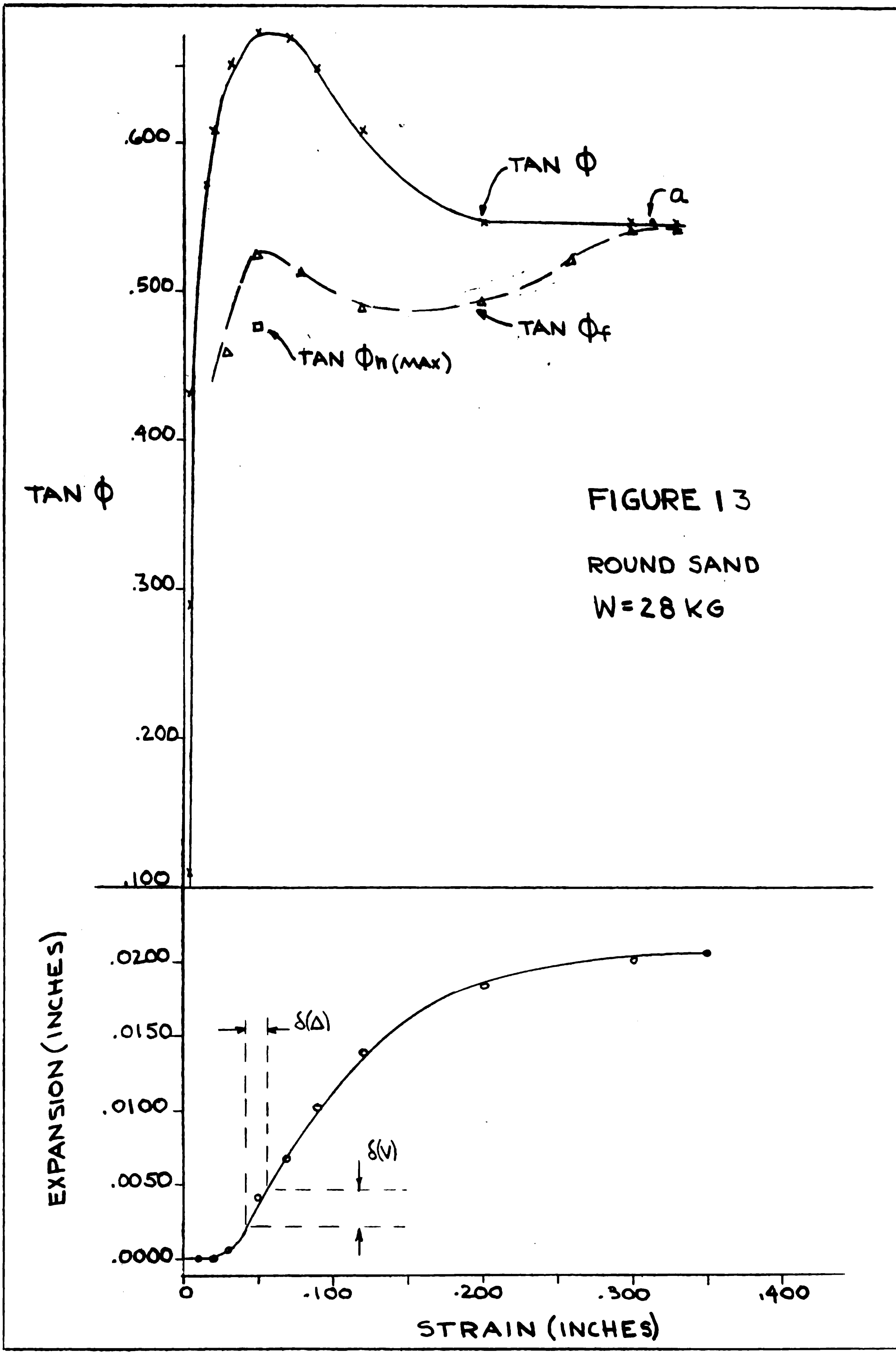

FIGURE 13

ROUND SAND

W=28 KG

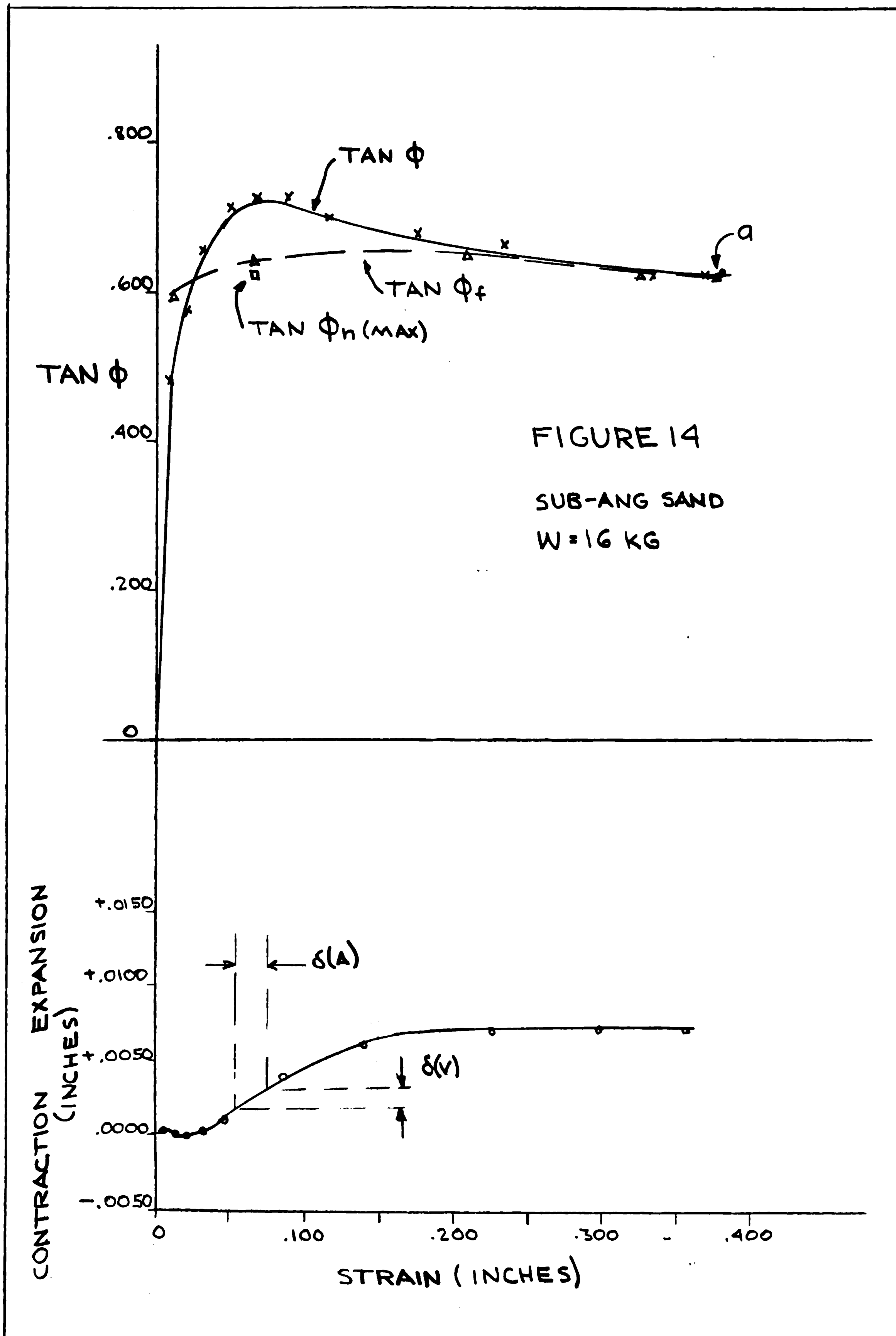

TAN Φ
.800
.600
.400
.200
0
TAN Φ
TAN Φf
TAN Φn (MAX)
a
FIGURE 14
SUB-ANG SAND
W = 16 KG
CONTRACTION EXPANSION (INCHES)
+.0150
+.0100
+.0050
.0000
−.0050
δ(A)
δ(V)
0
.100
.200
.300
.400
STRAIN (INCHES)

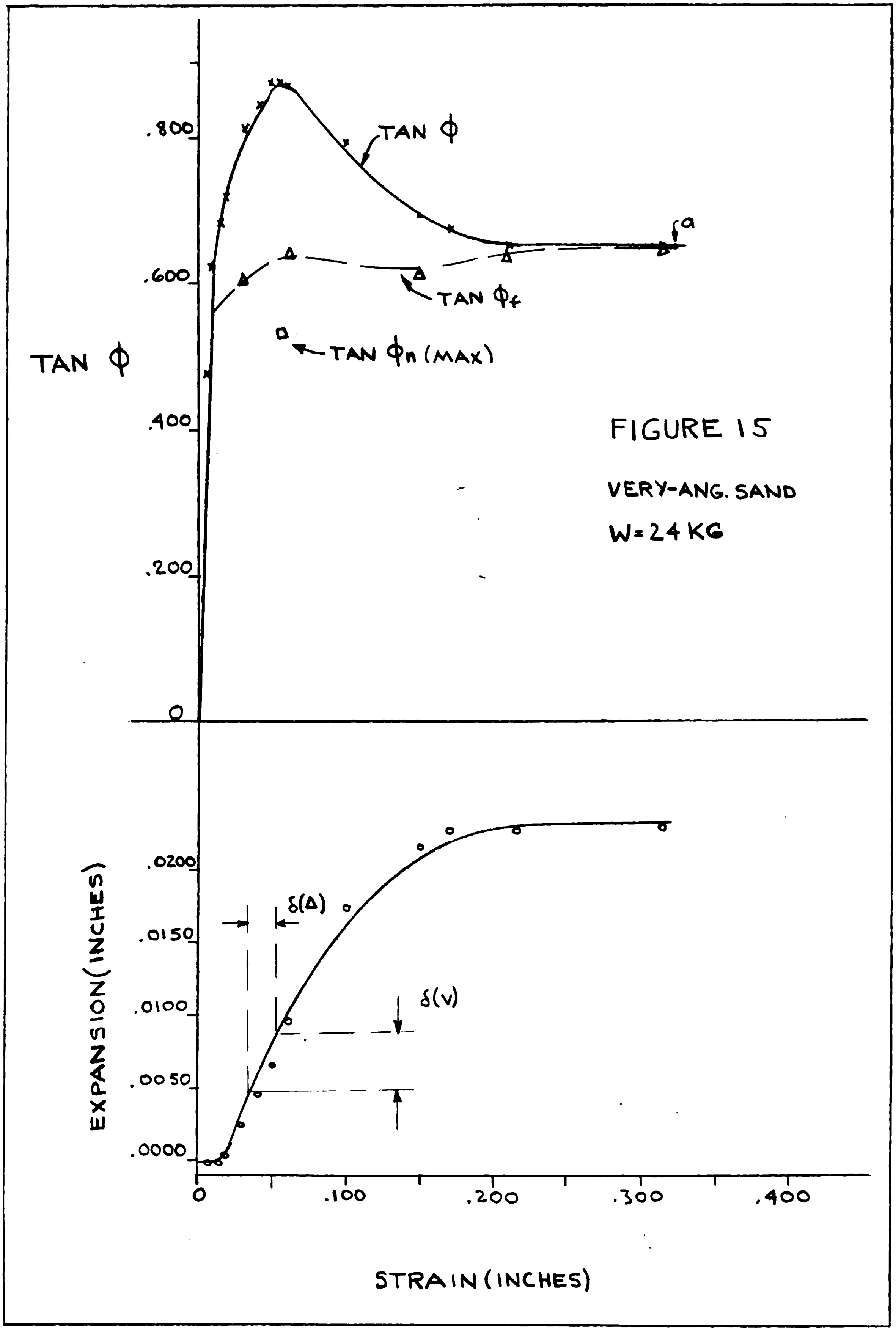

TAN Φ
TAN Φf
TAN Φn (MAX)
a
.800
.600
.400
.200
0
FIGURE 15
VERY-ANG. SAND
W=24 KG
EXPANSION (INCHES)
.0200
.0150
.0100
.0050
.0000
δ(Δ)
δ(V)
0
.100
.200
.300
.400
STRAIN (INCHES)

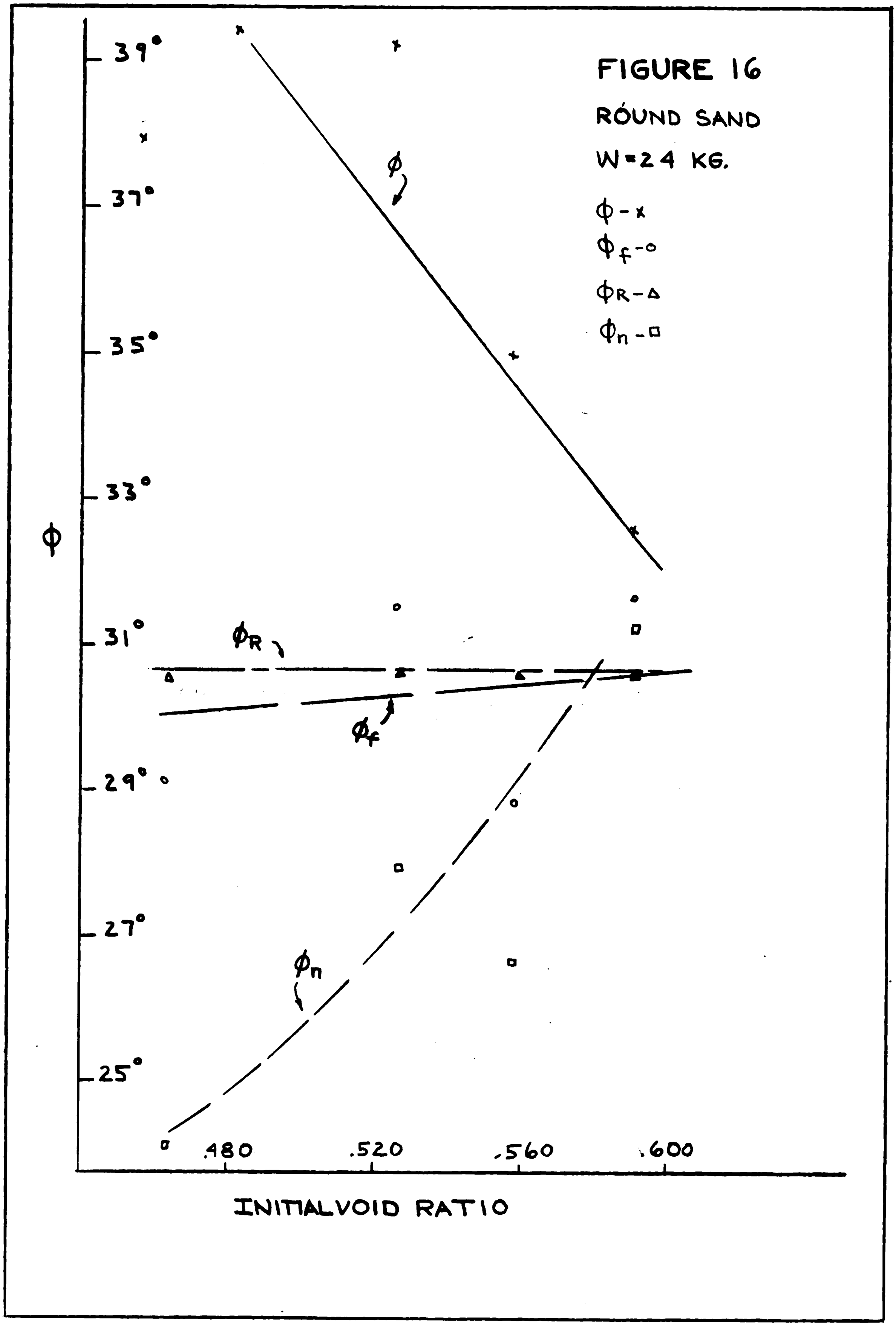
FIGURE 16
ROUND SAND
W=24 KG.
φ - x
φf - o
φR - Δ
φn - □
φ
φR
φf
φn
39°
37°
35°
33°
31°
29°
27°
25°
.480
.520
.560
.600
INITIAL VOID RATIO

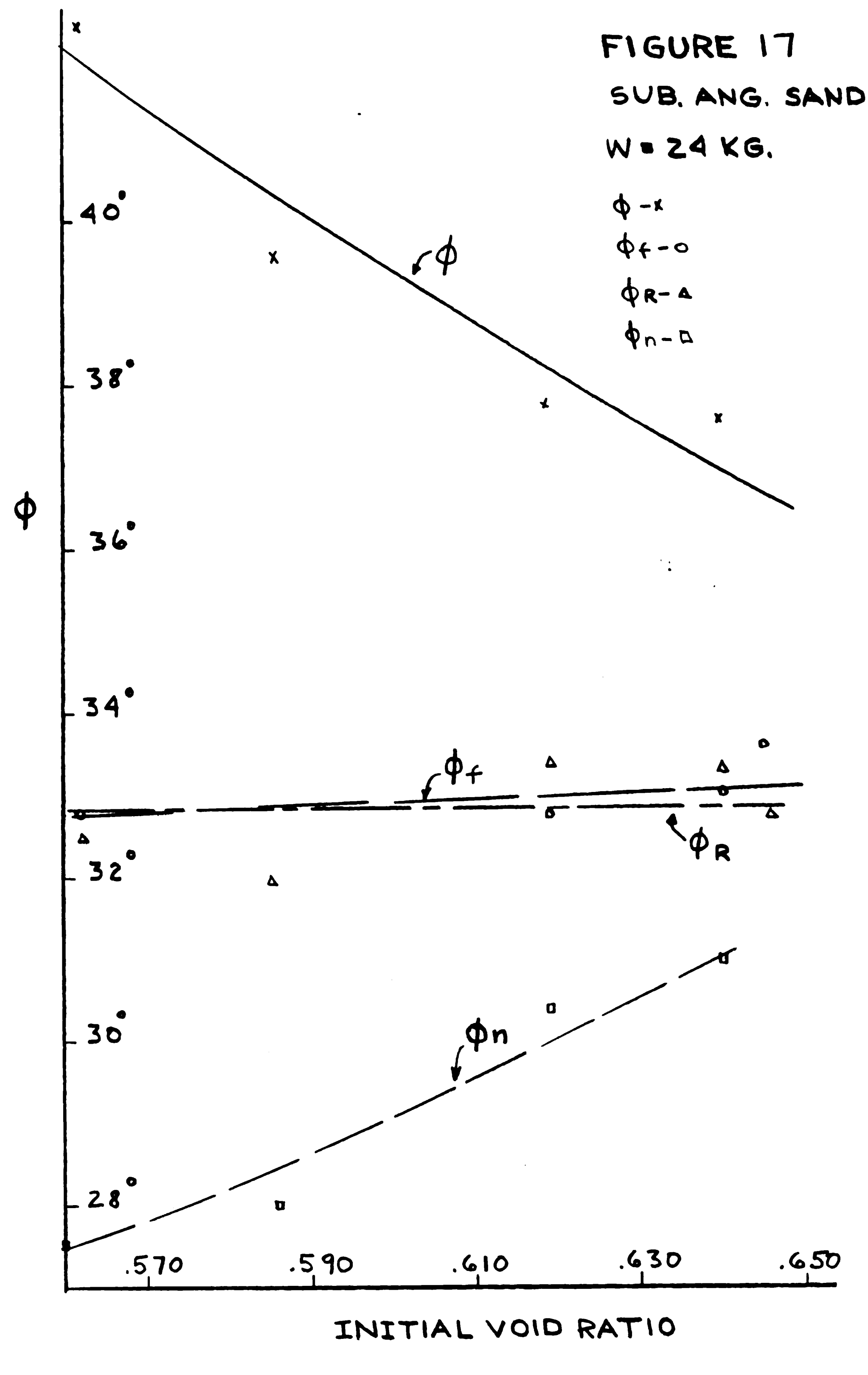
FIGURE 17
SUB. ANG. SAND
W = 24 KG.
φ - x
φf - o
φR - Δ
φn - □
φ
φf
φR
φn
40°
38°
36°
34°
32°
30°
28°
.570
.590
.610
.630
.650
INITIAL VOID RATIO

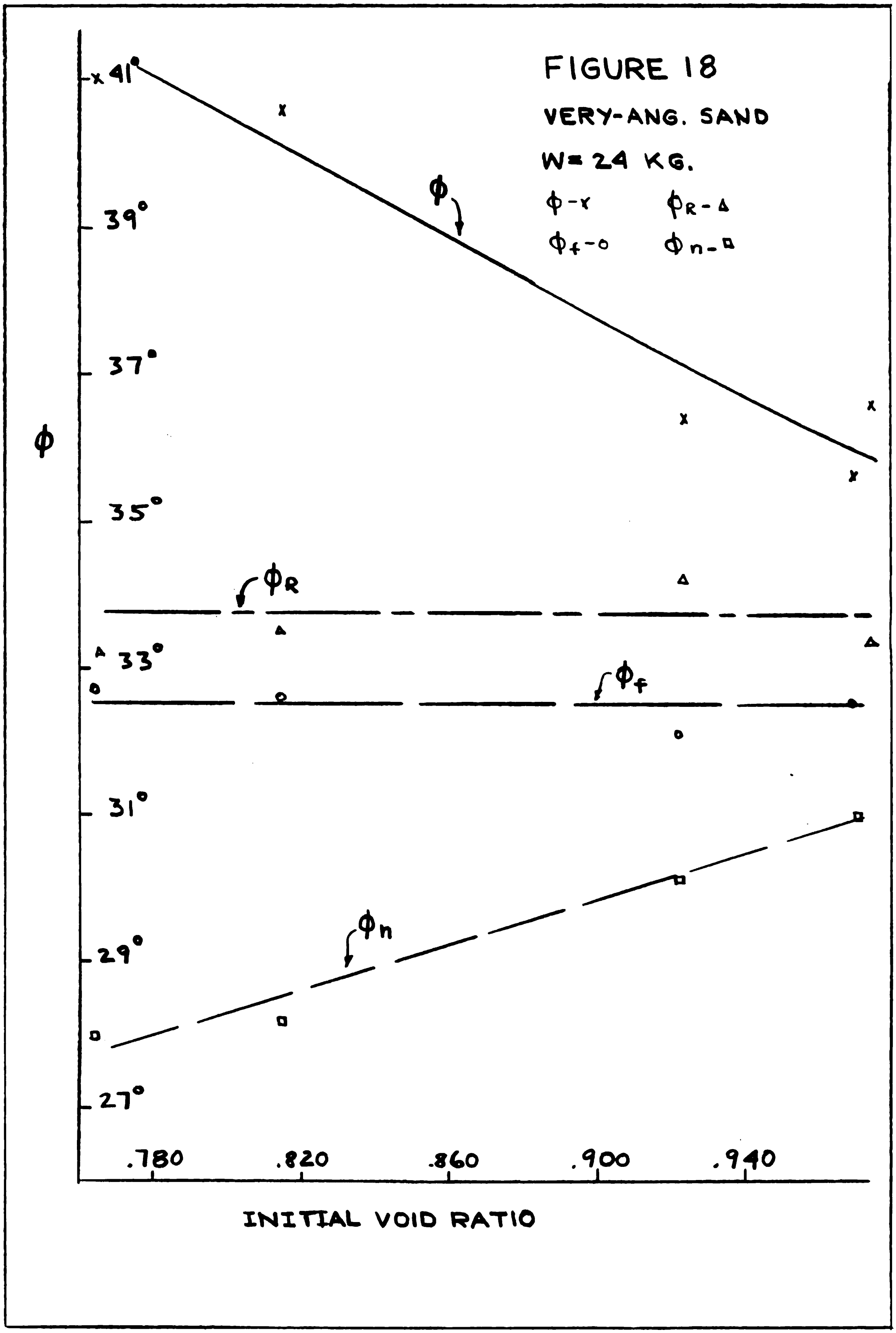
FIGURE 18
VERY-ANG. SAND
W= 24 KG.
φ-x φR-Δ
φf-o φn-□
φ
φR
φf
φn
41°
39°
37°
35°
33°
31°
29°
27°
.780
.820
.860
.900
.940
INITIAL VOID RATIO

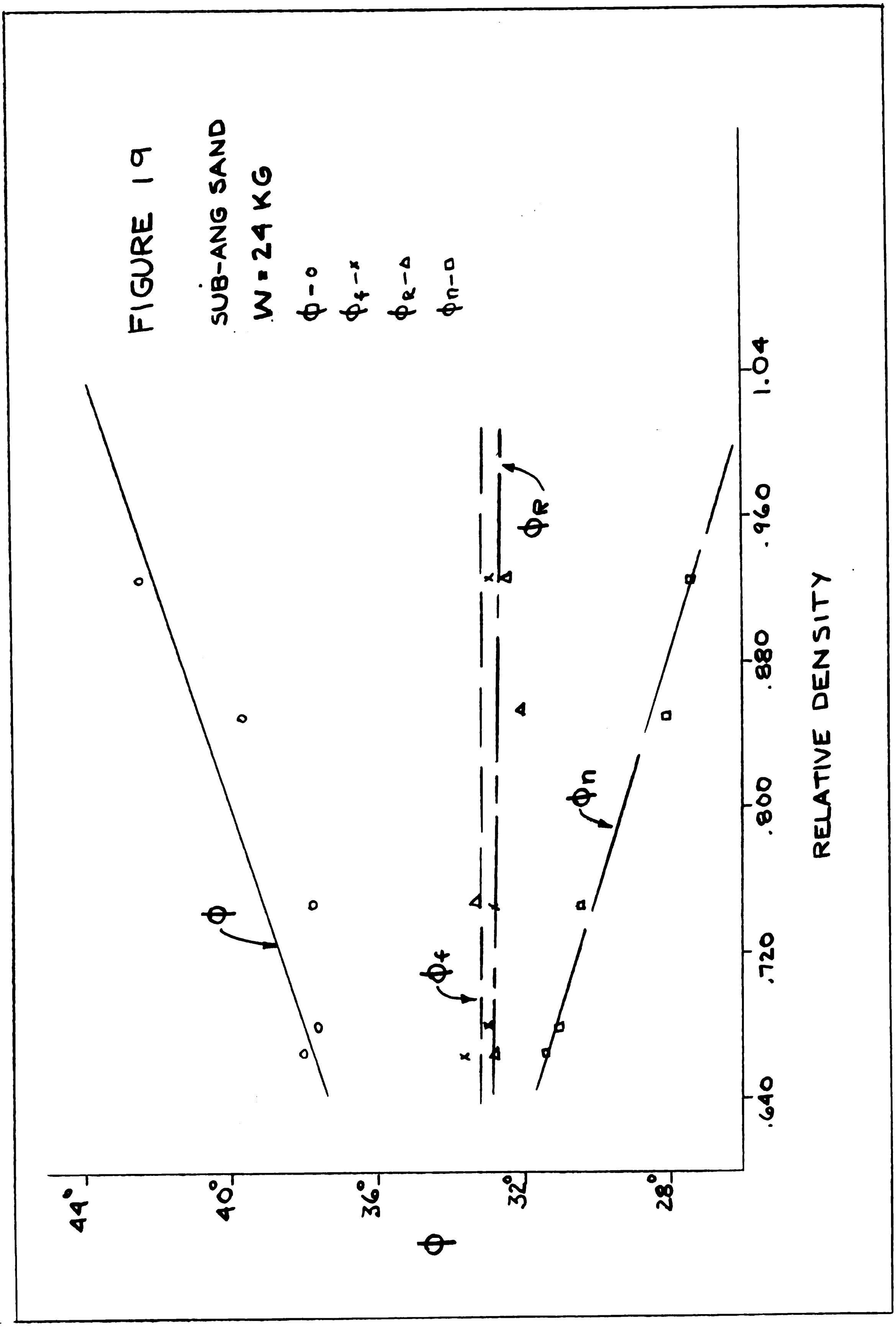
FIGURE 19
SUB-ANG SAND
W = 24 KG
ϕ - o
ϕ_f - x
ϕ_R - △
ϕ_n - □
ϕ
ϕ_f
ϕ_R
ϕ_n
44°
40°
36°
32°
28°
.640
.720
.800
.880
.960
1.04
RELATIVE DENSITY

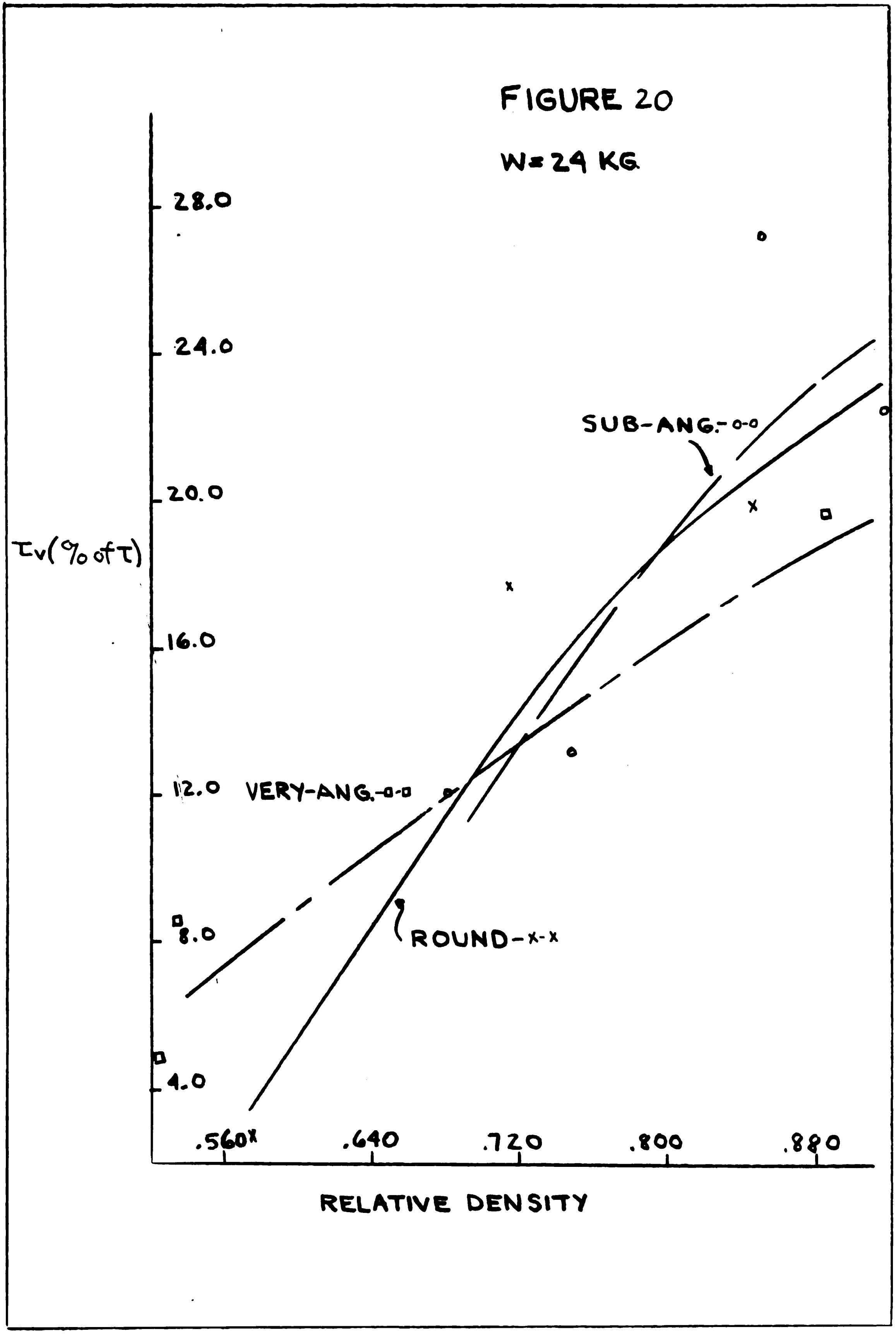
FIGURE 20
W=24 KG
28.0
24.0
20.0
16.0
12.0
8.0
4.0
Tv(% of T)
SUB-ANG.-o-o
VERY-ANG.-□-□
ROUND-x-x
.560
.640
.720
.800
.880
RELATIVE DENSITY

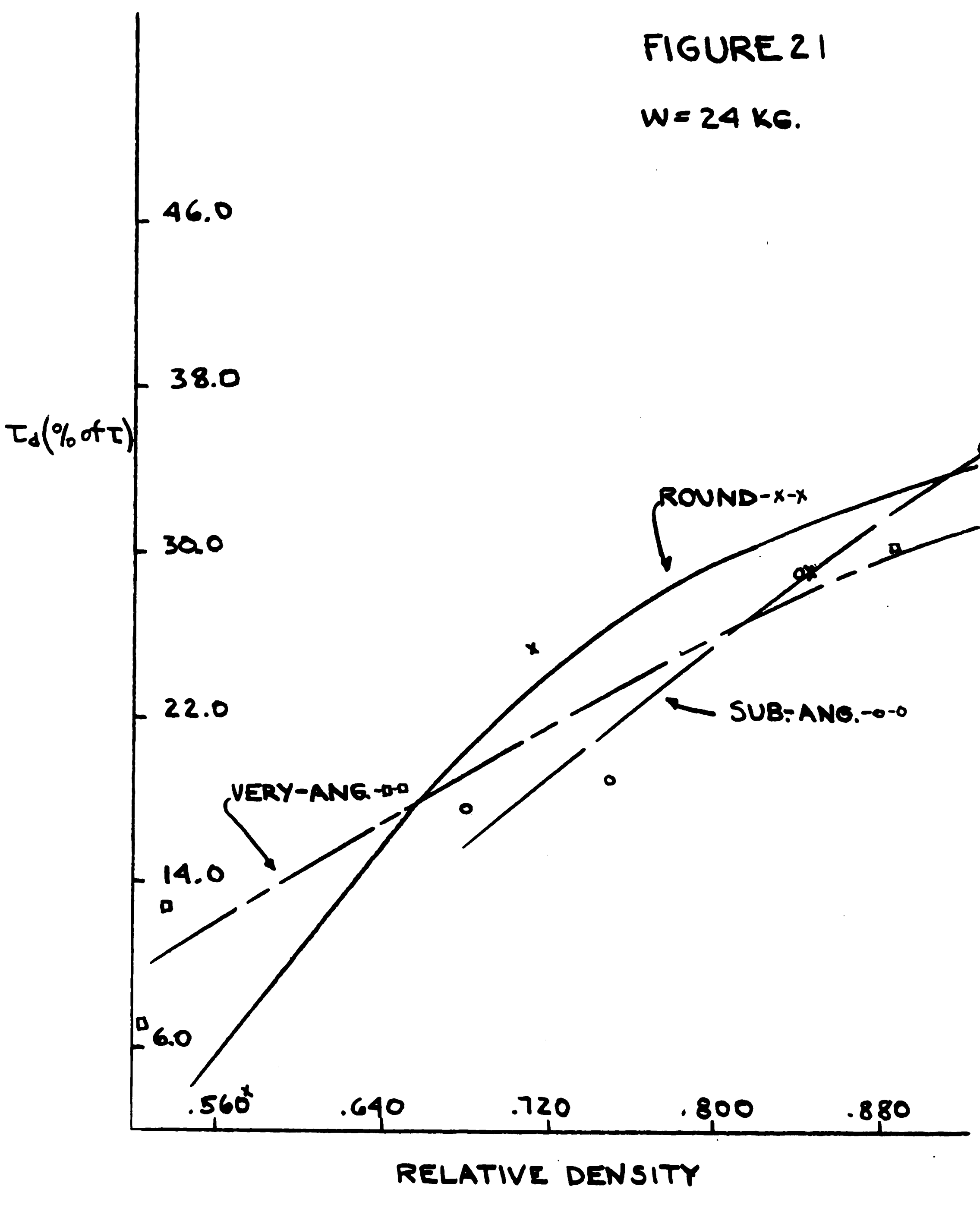

FIGURE 21
W = 24 KG.
46.0
38.0
30.0
22.0
14.0
6.0
τd (% of τ)
ROUND-x-x
SUB-ANG.-o-o
VERY-ANG.-□-□
.560
.640
.720
.800
.880
RELATIVE DENSITY

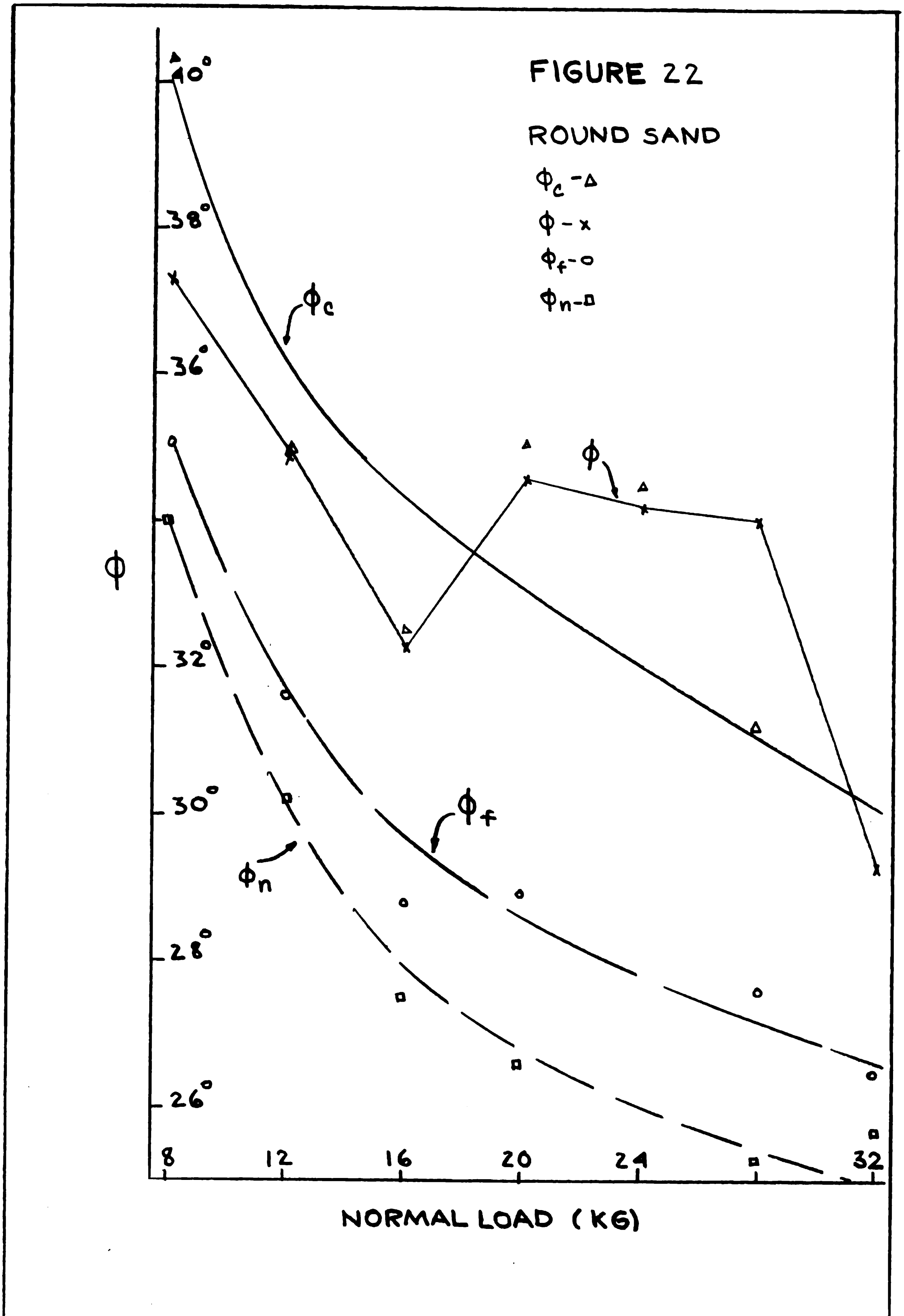

FIGURE 22
ROUND SAND
ϕ_c - Δ
ϕ - x
ϕ_f - o
ϕ_n - □
ϕ_c
ϕ
ϕ_f
ϕ_n
ϕ
40°
38°
36°
32°
30°
28°
26°
8
12
16
20
24
32
NORMAL LOAD (KG)

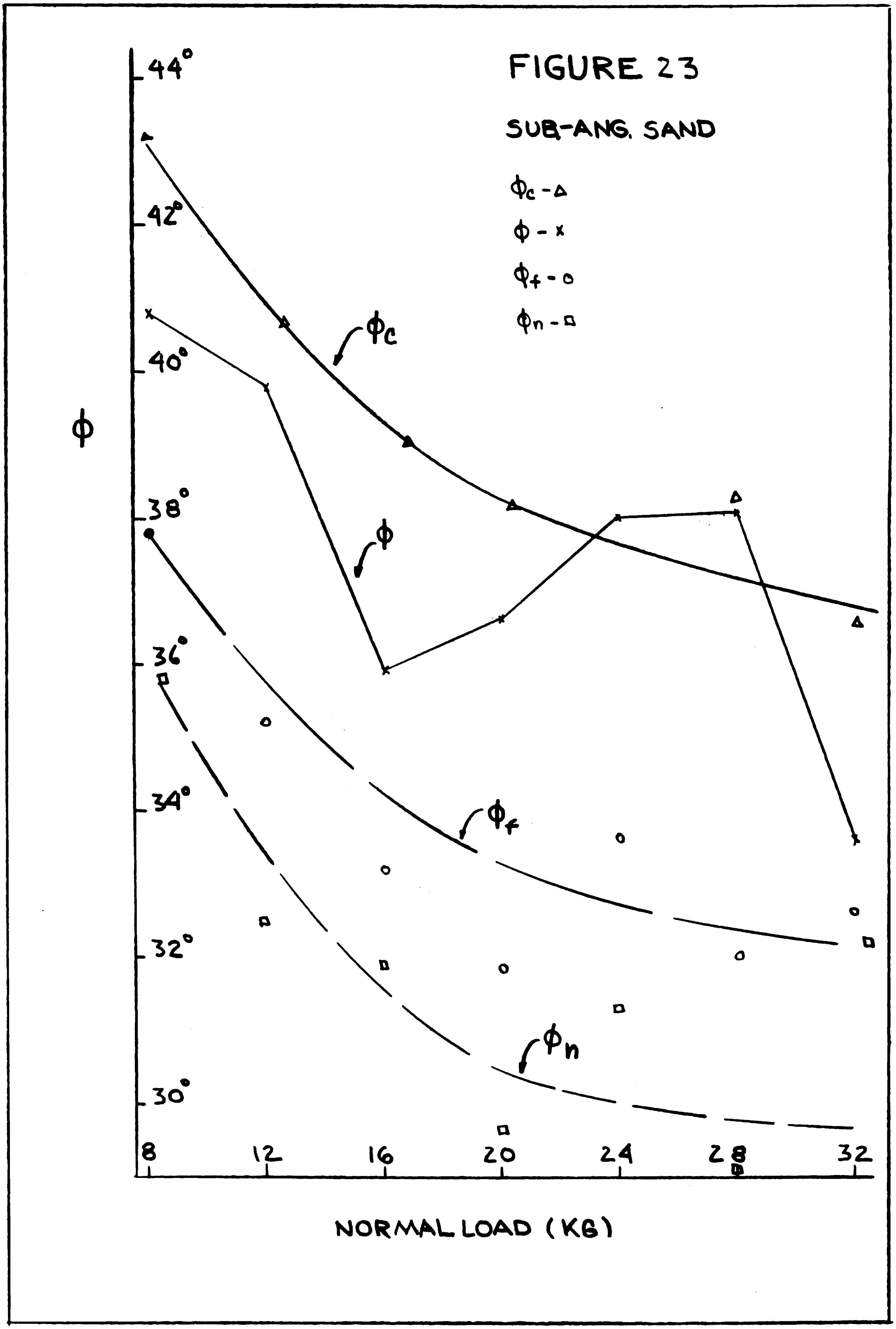
FIGURE 23
SUB-ANG. SAND
φc - Δ
φ - x
φf - o
φn - □
φ
φc
φ
φf
φn
44°
42°
40°
38°
36°
34°
32°
30°
8
12
16
20
24
28
32
NORMAL LOAD (KG)

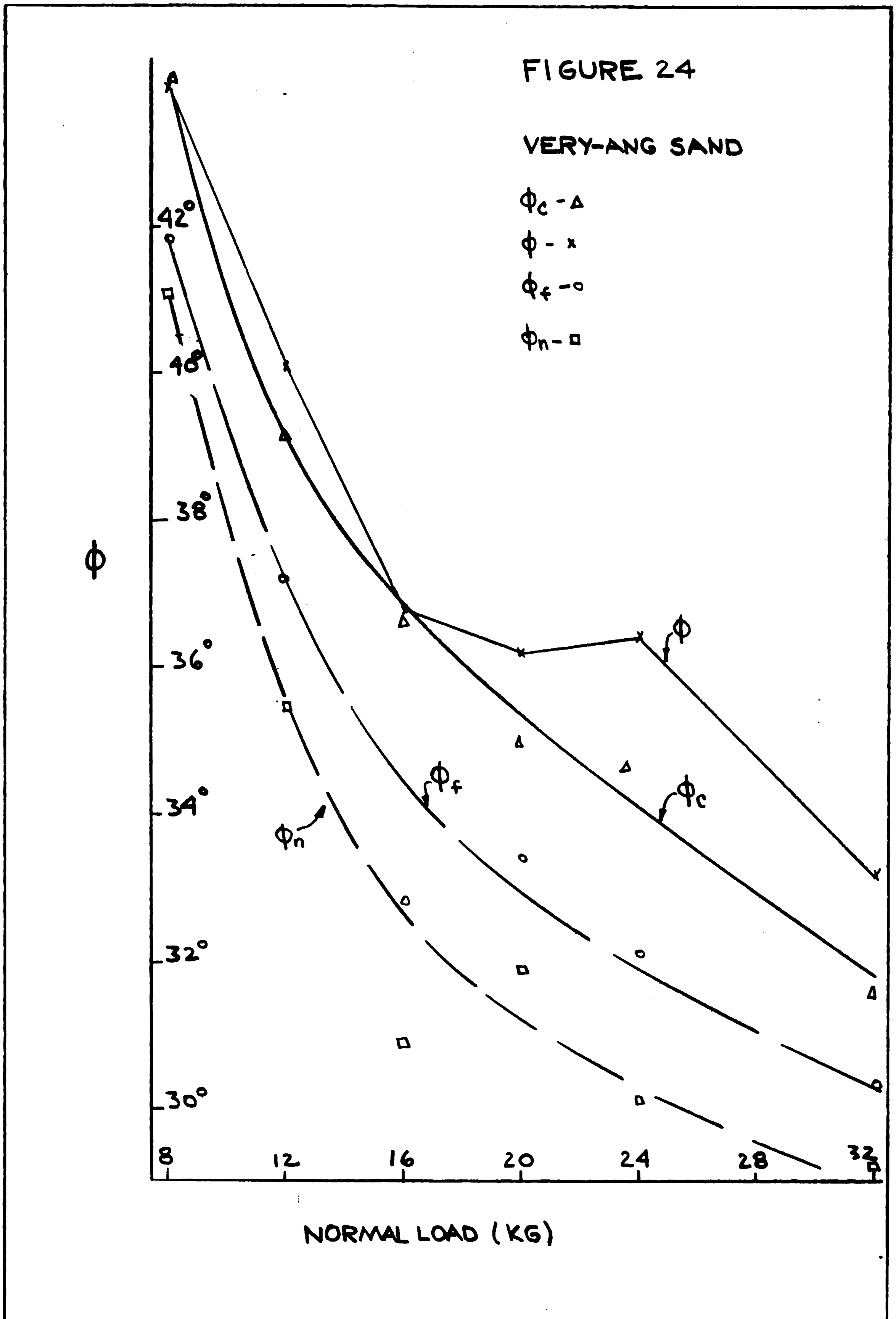
FIGURE 24
VERY-ANG SAND
ϕ_c - Δ
ϕ - x
ϕ_f - o
ϕ_n - □
ϕ
42°
40°
38°
36°
34°
32°
30°
8
12
16
20
24
28
32
ϕ
ϕ_c
ϕ_f
ϕ_n
NORMAL LOAD (KG)

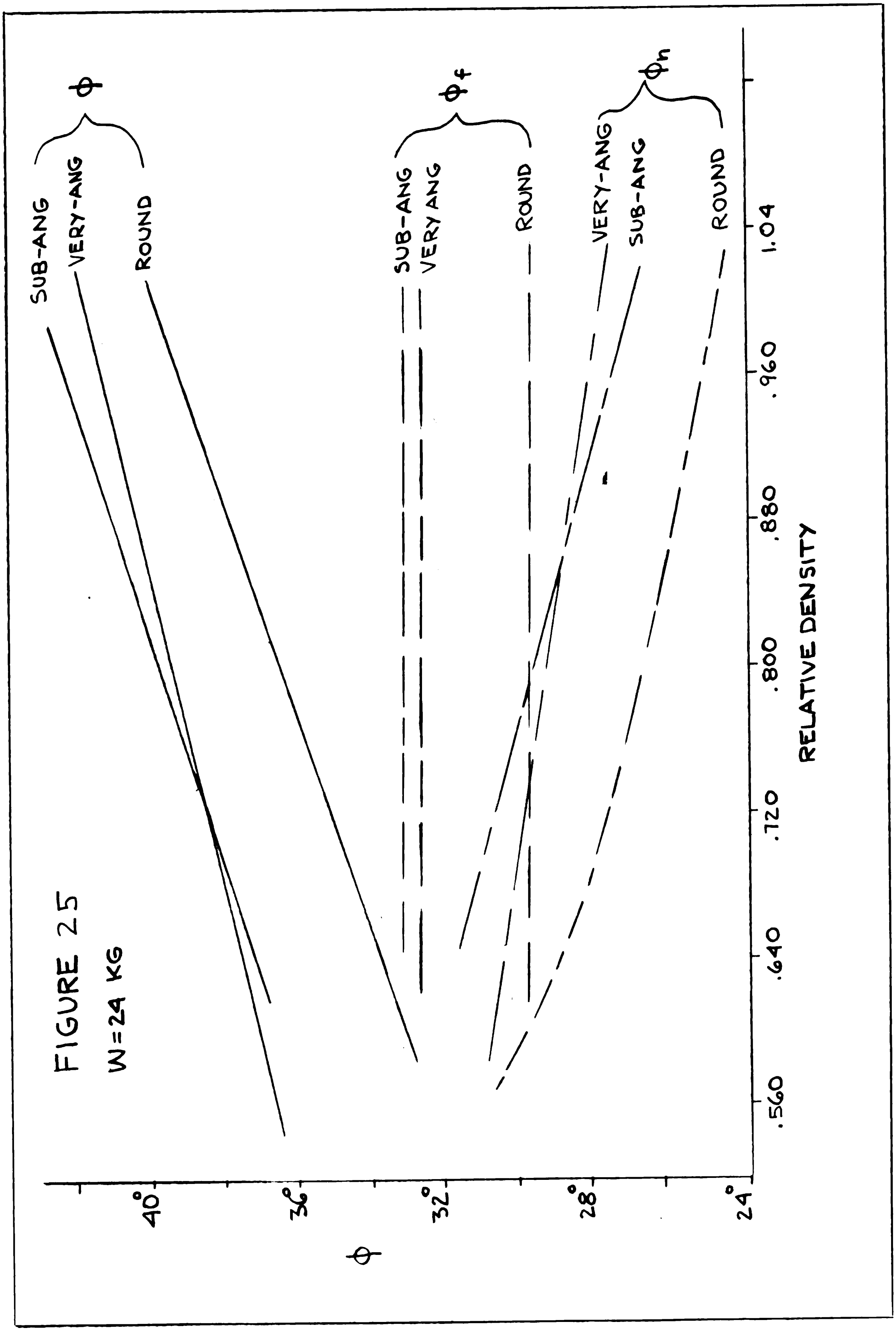

FIGURE 25
W=24 KG

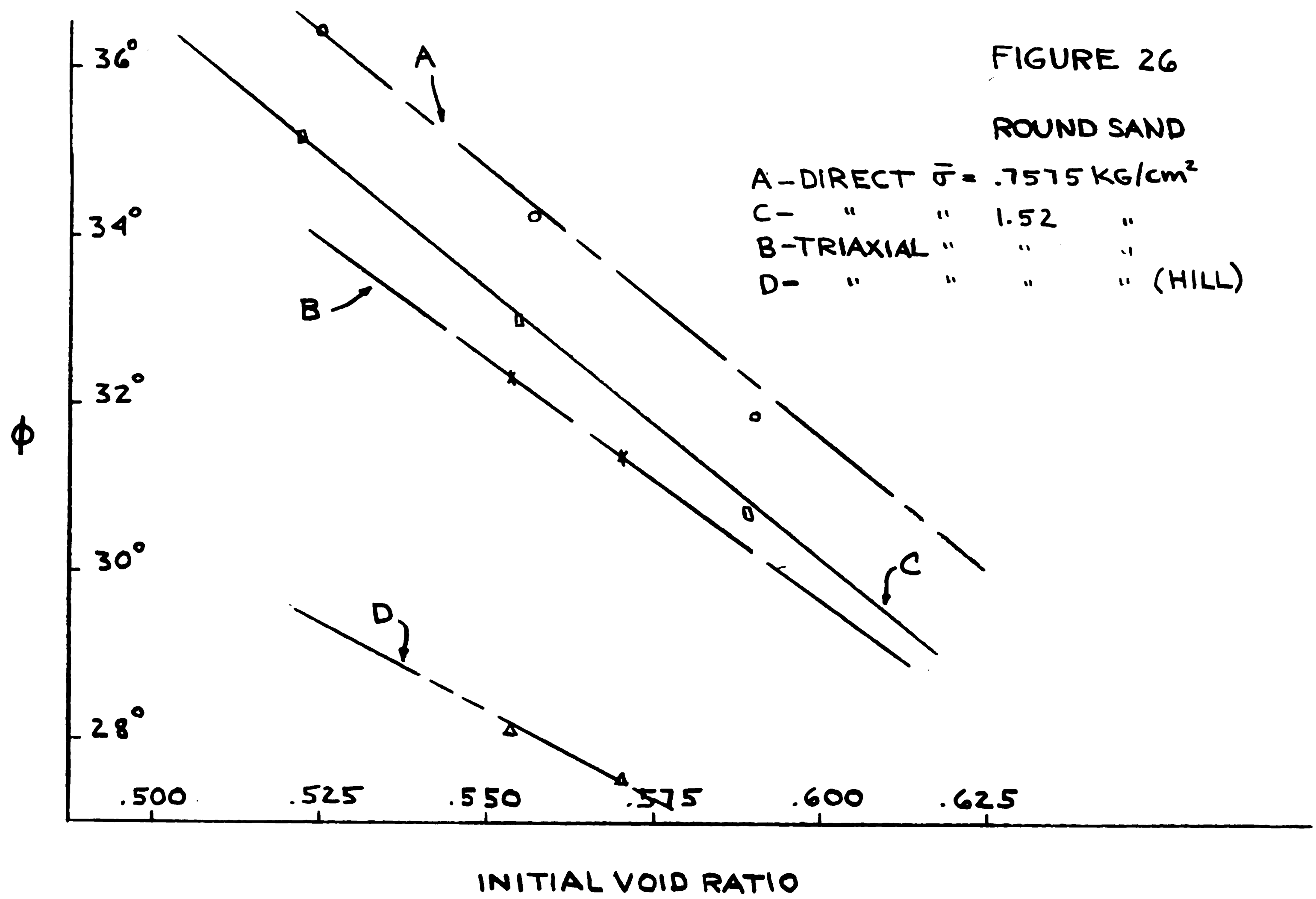
ROUND SAND
A–DIRECT $\bar{\sigma}$ = .7575 KG/cm²
C– " " 1.52 "
B–TRIAXIAL " " "
D– " " " " (HILL)
A
B
C
D
36°
34°
32°
30°
28°
ϕ
.500
.525
.550
.575
.600
.625
INITIAL VOID RATIO

FIGURE 26

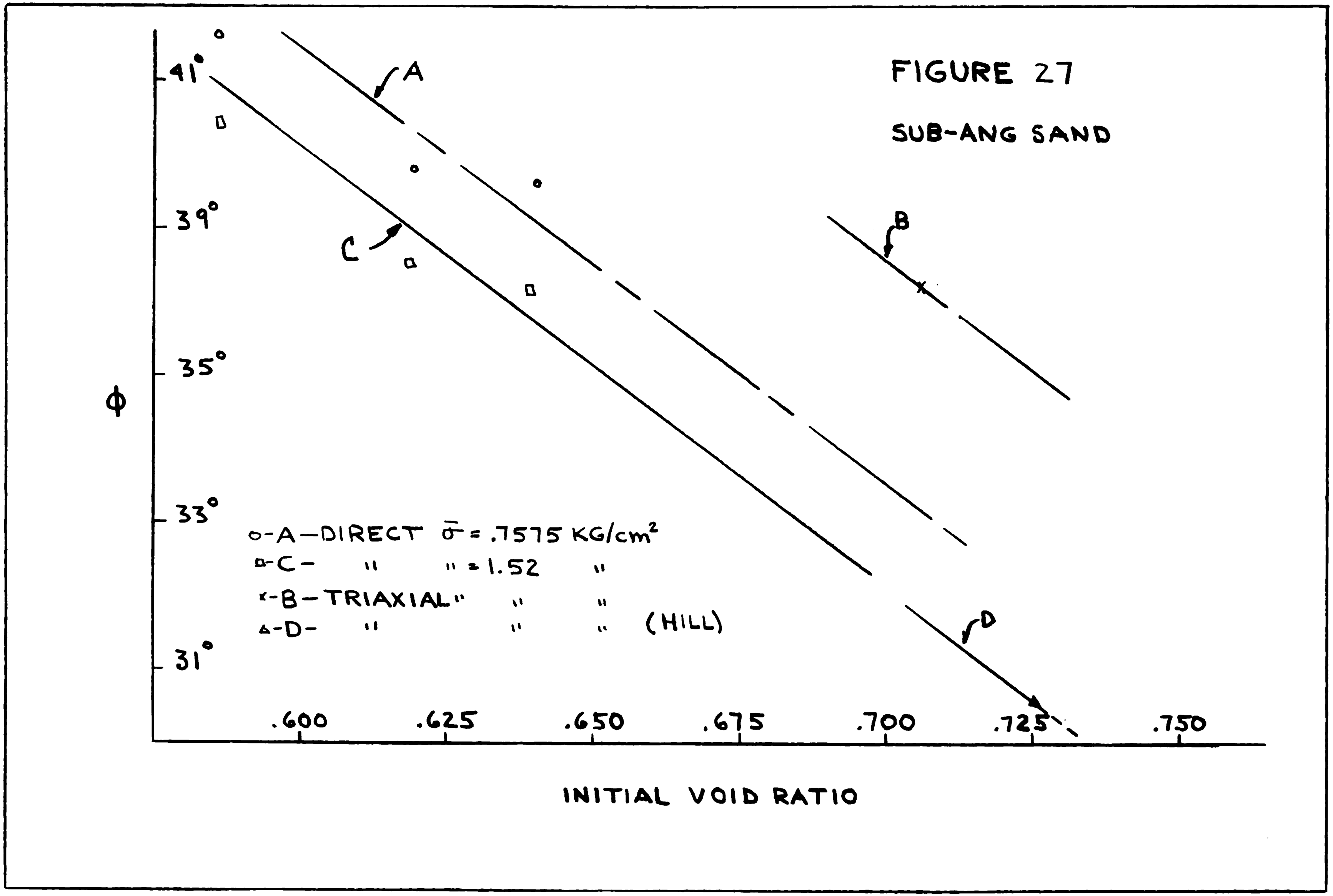
FIGURE 27
SUB-ANG SAND
41°
39°
35°
33°
31°
Φ
A
B
C
D
○-A—DIRECT $\bar{\sigma}$ = .7575 KG/cm²
□-C- " " = 1.52 "
×-B—TRIAXIAL " " "
△-D- " " " (HILL)
.600
.625
.650
.675
.700
.725
.750
INITIAL VOID RATIO

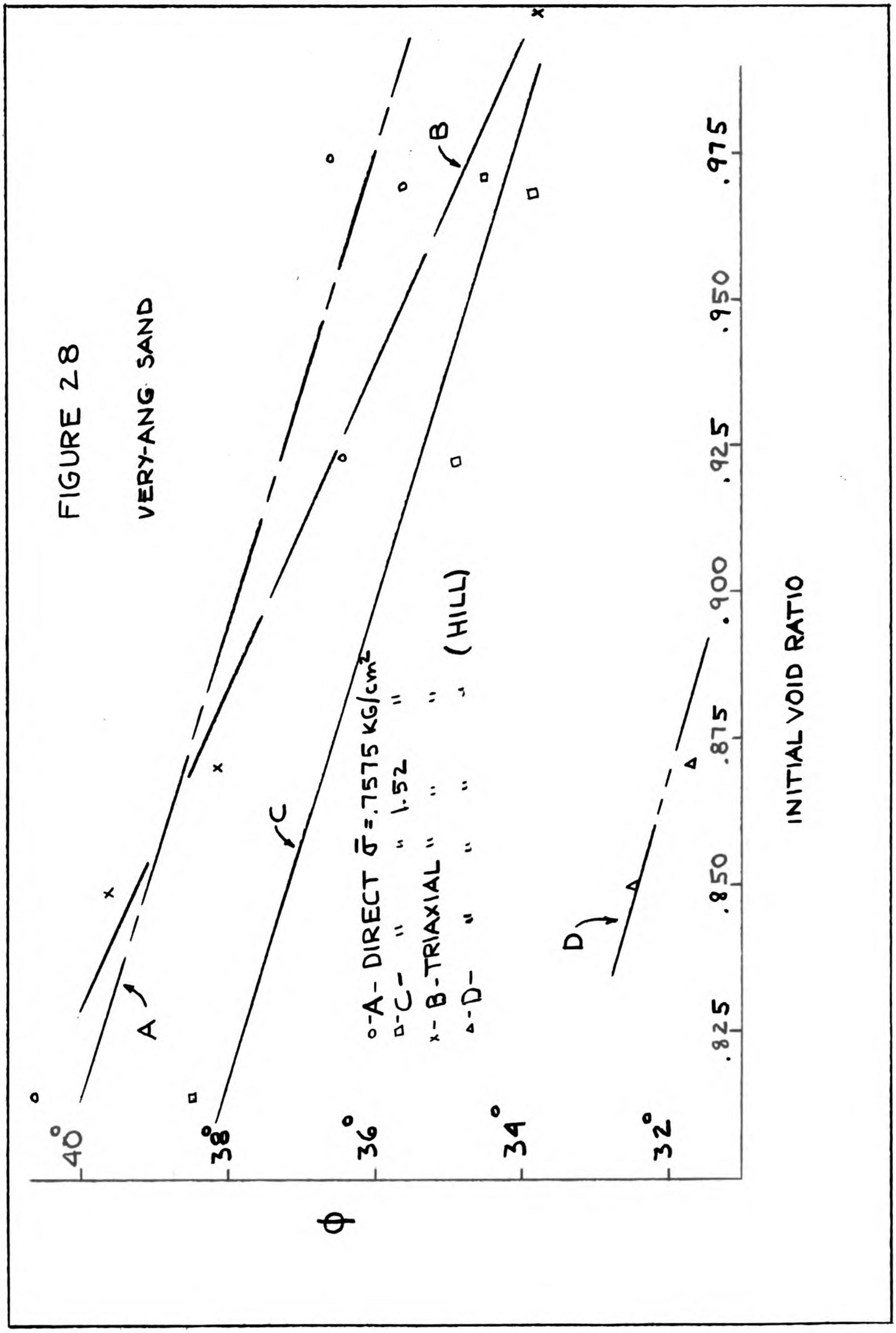
FIGURE 28
VERY-ANG SAND
o-A- DIRECT $\bar{\sigma}$ = .7575 KG/cm²
□-C- " 1.52
x- B-TRIAXIAL " "
△-D- " " "
(HILL)
A
B
C
D
40°
38°
36°
34°
32°
φ
.825
.850
.875
.900
.925
.950
.975
INITIAL VOID RATIO

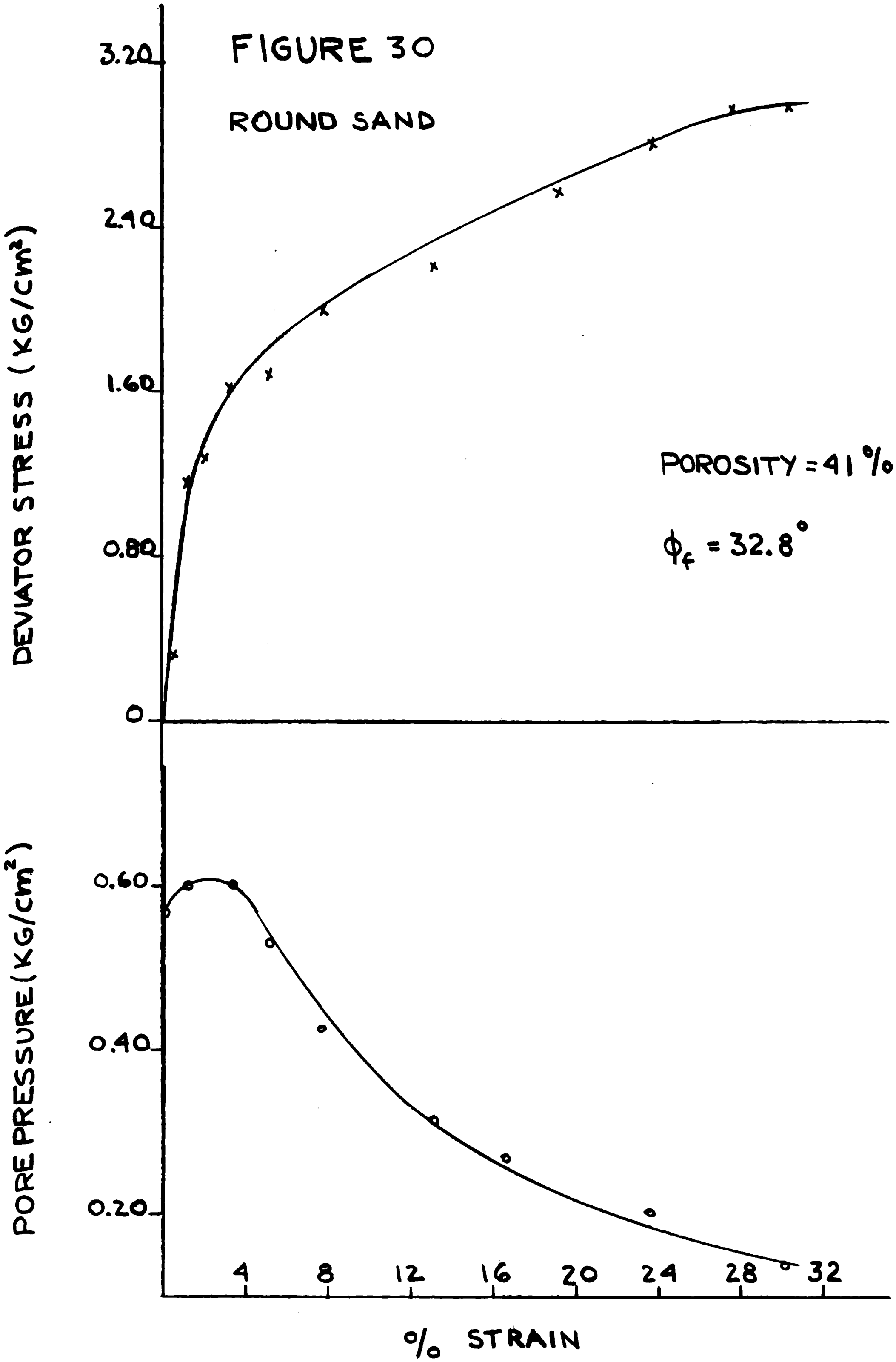
FIGURE 30
ROUND SAND
DEVIATOR STRESS (KG/CM²)
3.20
2.40
1.60
0.80
0
POROSITY = 41 %
ϕ_f = 32.8°
PORE PRESSURE (KG/CM²)
0.60
0.40
0.20
4
8
12
16
20
24
28
32
% STRAIN

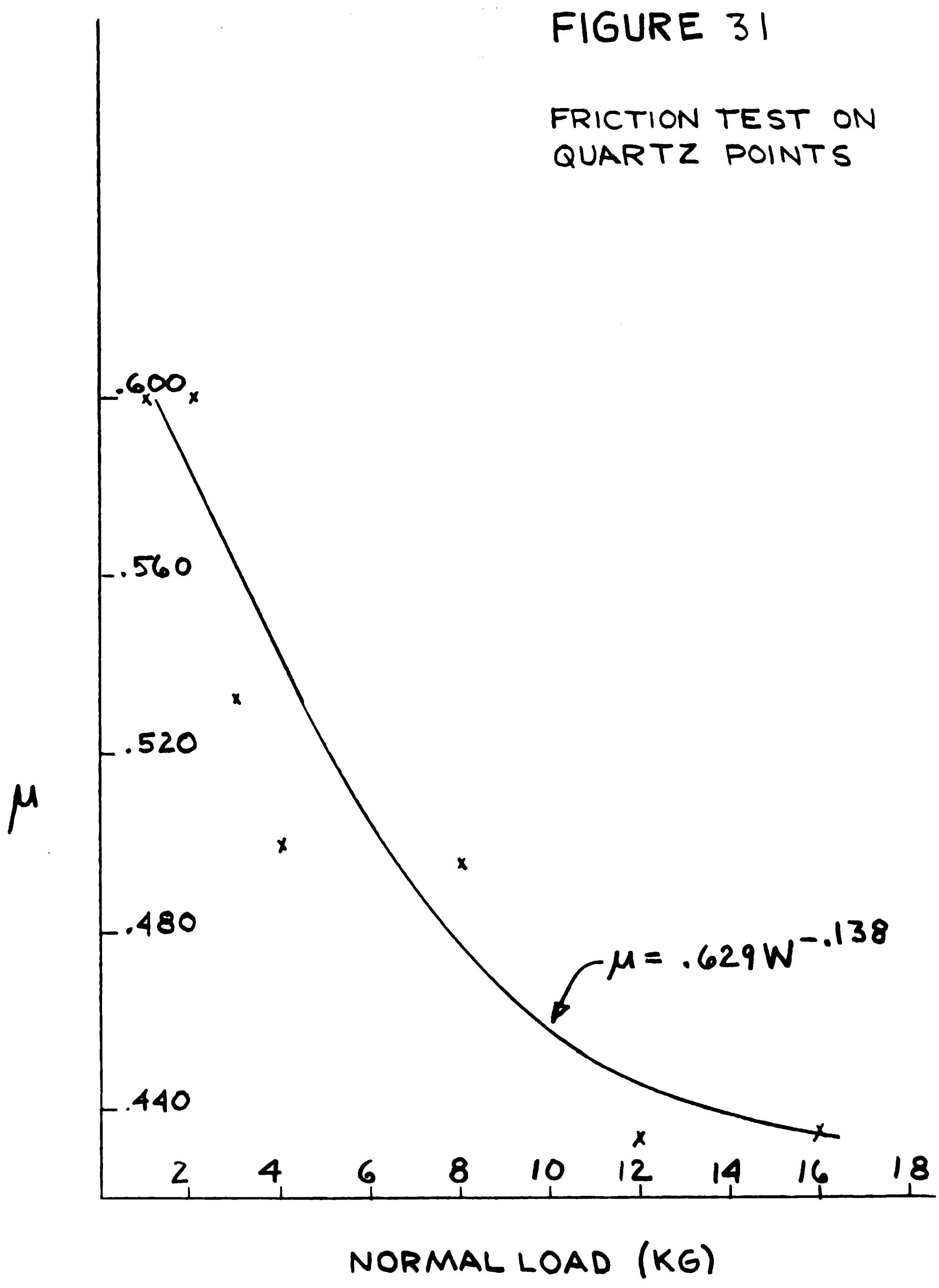
FIGURE 31
FRICTION TEST ON QUARTZ POINTS
.600
.560
.520
.480
.440
μ
$\mu = .629W^{-.138}$
2 4 6 8 10 12 14 16 18
NORMAL LOAD (KG)

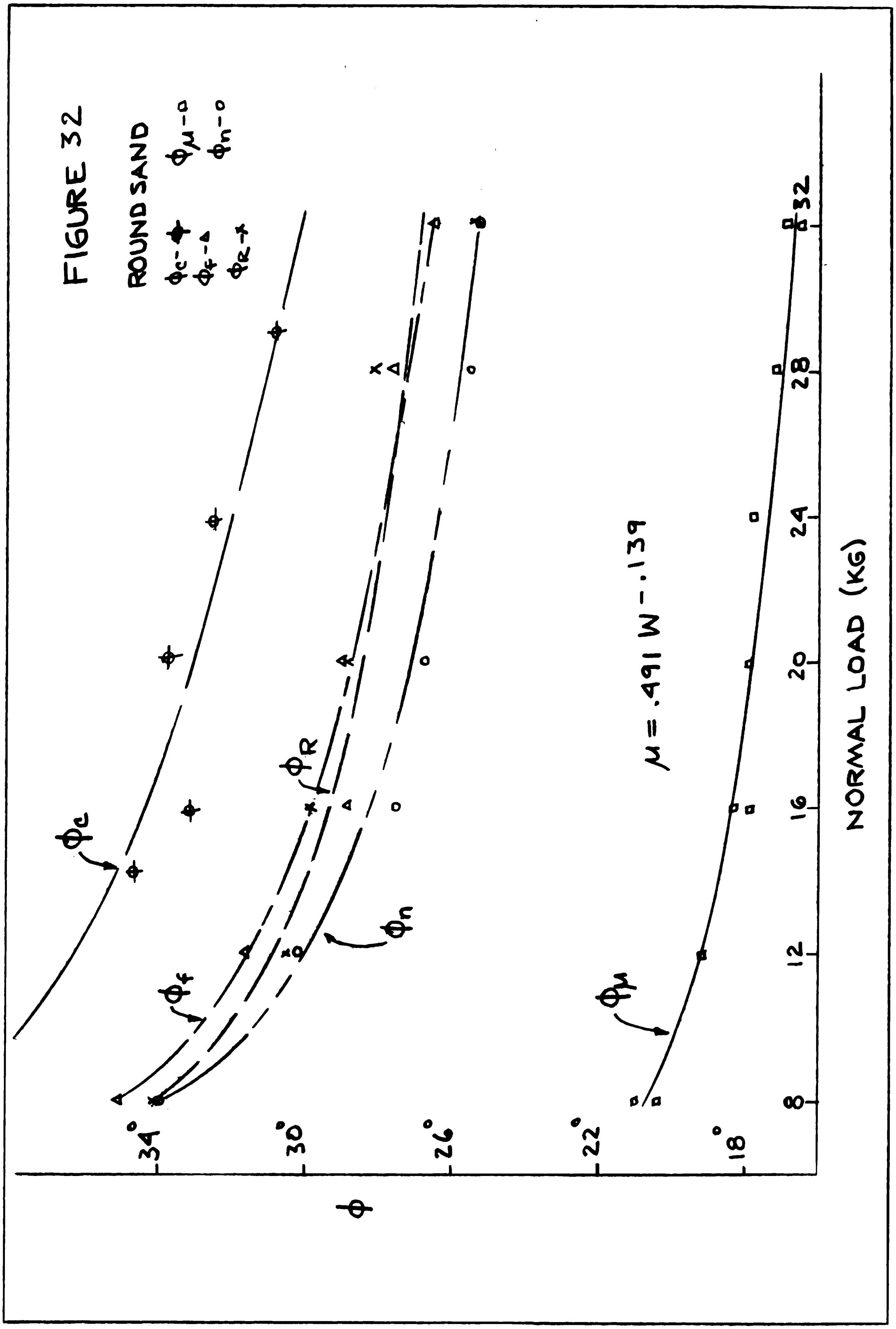

FIGURE 32
ROUND SAND
ϕ_c - ✦
ϕ_f - △
ϕ_R - x
ϕ_μ - □
ϕ_n - o
ϕ_c
ϕ_f
ϕ_R
ϕ_n
ϕ_μ
$\mu = .491\,W^{-.139}$
ϕ
34°
30°
26°
22°
18°
8
12
16
20
24
28
32
NORMAL LOAD (KG)

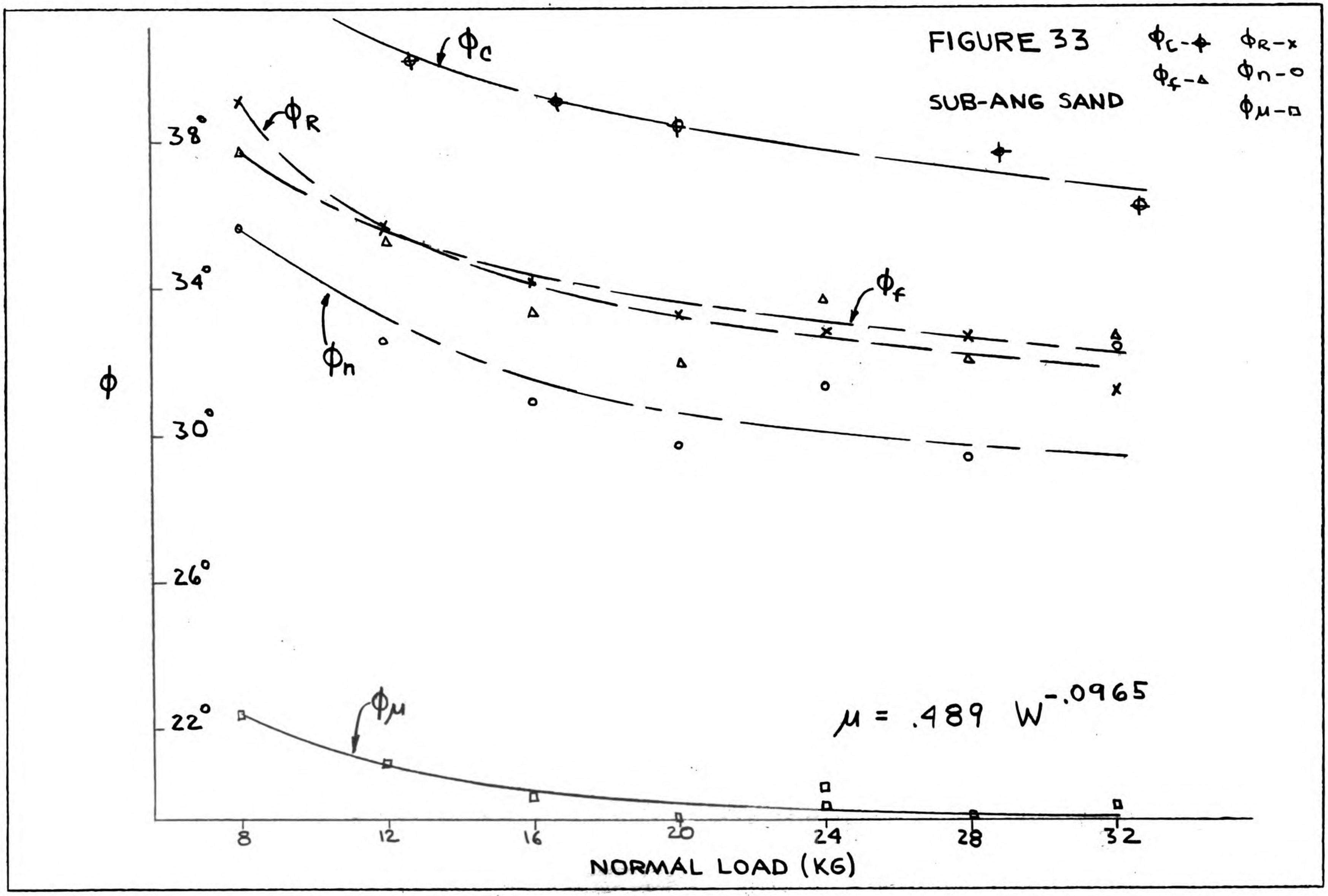

FIGURE 33

SUB-ANG SAND

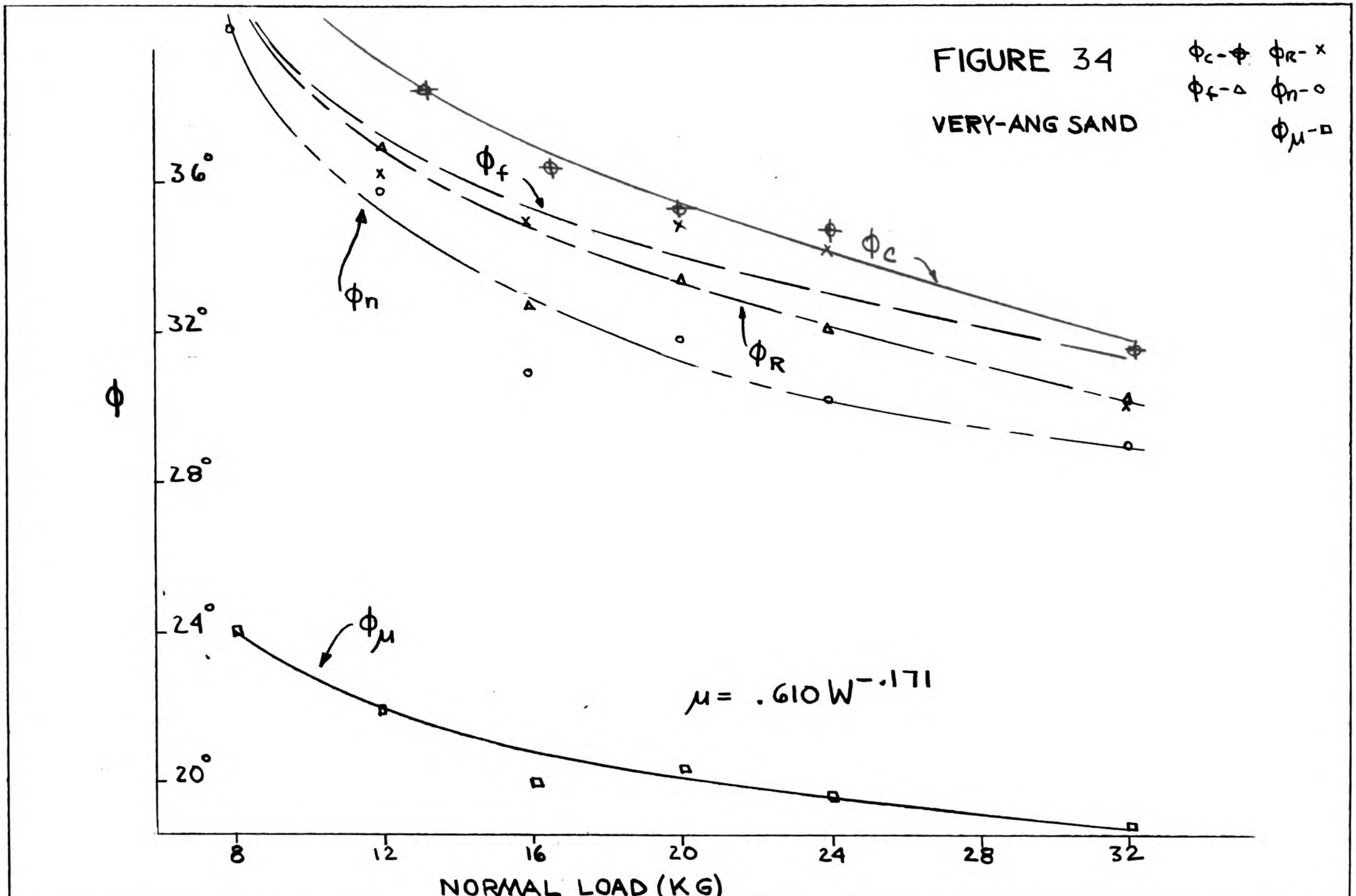
FIGURE 34
VERY-ANG SAND
ϕ_c - ⊕ ϕ_R - x
ϕ_f - △ ϕ_n - o
ϕ_μ - □
ϕ_f
ϕ_c
ϕ_n
ϕ_R
ϕ_μ
$\mu = .610 W^{-.171}$
ϕ
36°
32°
28°
24°
20°
8
12
16
20
24
28
32
NORMAL LOAD (KG)

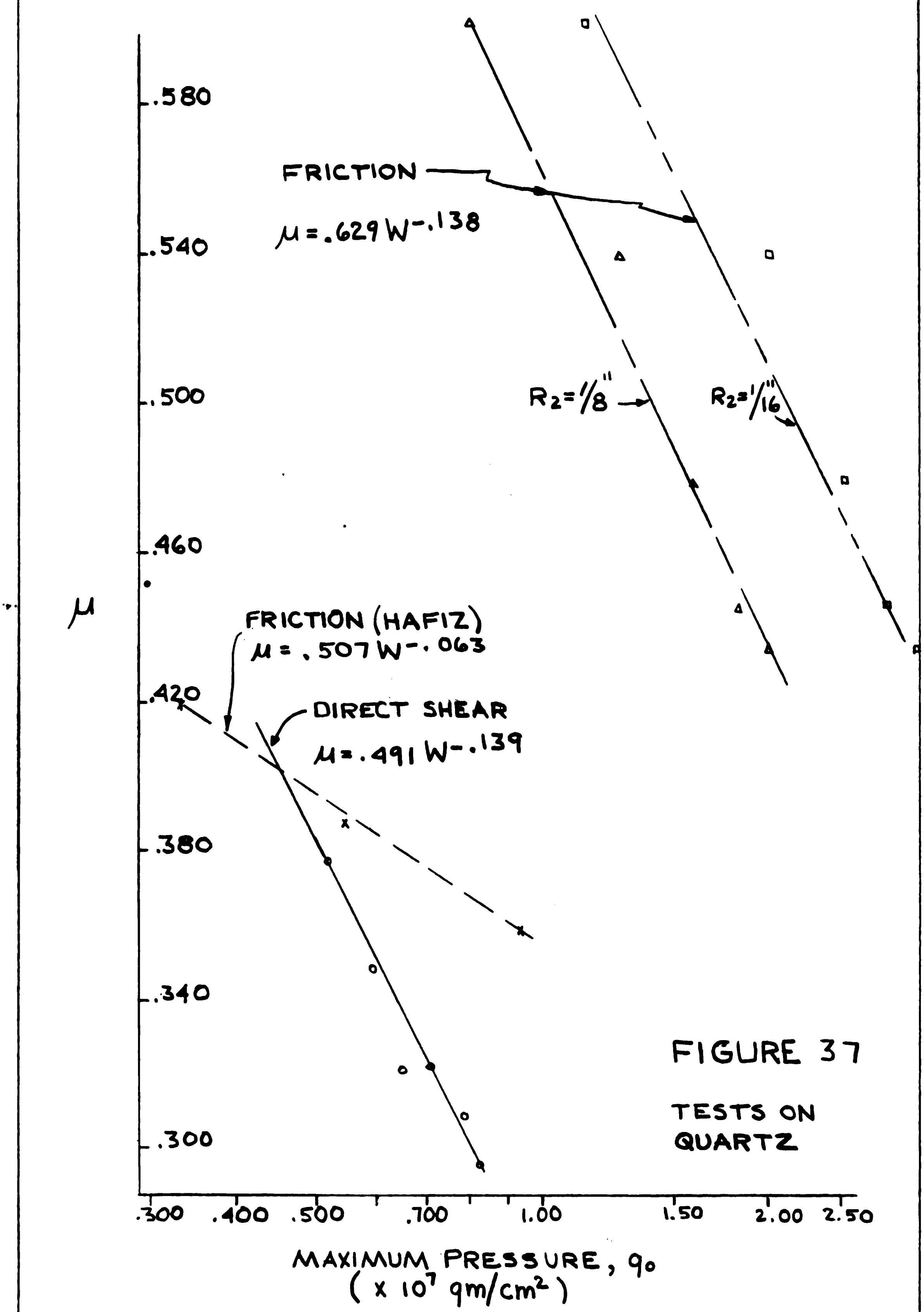

FIGURE 37

TESTS ON QUARTZ

SAND	SIEVE SIZE	e_{max}	e_{min}
Round	30-50	.7575	.488
Sub-Angular	30-50	.854	.539
Very-Angular	30-50	1.204	.763

TABLE I MAXIMUM AND MINIMUM VOID RATIO

TEST #	e_o	W(Kg)	ϕ°	ϕ_f°	ϕ_n°	ϕ_R°	μ	Δm (INCHES)
				DRY TESTS				
Round Sand								
5	.615	8	37.3	35.1	34.0	34.0	.384	.060
16	.564	12	35.0	31.6	30.2	30.2	.349	.055
1	.504	16	32.3	28.8	27.5	29.9	.322	.080
10	.578	20	34.6	28.9	26.6	28.8	.322	.090
19	.521	28	34.0	27.6	25.3	28.1	.309	.050
3	.508	32	29.3	26.5	25.7	25.4	.297	.045
Sub-Angular Sand								
7	.724	8	40.8	37.8	35.8	39.1	.410	.080
17	.683	12	39.8	35.2	32.5	35.6	.385	.050
8	.770	16	35.9	33.2	31.9	34.2	.366	.070
11	.699	20	36.6	31.8	29.6	33.2	.352	.070
13	.645	24	38.0	33.6	31.3	32.8	.370	.050
20	.665	28	38.1	32.0	29.1	32.6	.354	.070
9	.736	32	33.6	32.6	32.2	31.1	.360	.070

TABLE II DIRECT SHEAR TESTS ON SAND TYPE A-W VARIED

TEST #	e_o	W(Kg)	ϕ°	ϕ_f°	ϕ_n°	ϕ_R°	μ	Δm(INCH)
Very-Angular Sand								
6	1.03	8	43.9	41.8	40.1	42.0	.445	.150
18	.939	12	40.1	37.2	35.4	36.3	.403	.080
2	1.01	16	36.8	32.8	30.9	35.0	.362	.080
12	1.04	20	36.2	33.4	31.9	34.8	.368	.100
15	.923	24	36.4	32.1	30.1	34.2	.355	.080
4	0.892	32	33.3	30.3	29.2	30.1	.337	.110
				SATURATED TESTS				
Round Sand								
3-S	.525	8	41.2	33.8	29.7	36.0	.372	.035
1-S	.598	16	34.5	29.7	27.9	30.3	.330	.045
2-S	.550	32	33.5	27.1	25.0	28.6	.304	.040

TABLE II Continued DIRECT SHEAR TESTS ON SAND TYPE A-W VARIED

TEST #	e_o	ϕ°	ϕ_f°	ϕ_n°	ϕ_R°	μ	Δm (INCHES)
			DRY TESTS - W = 24 Kg				
Round Sand							
26A	.590	31.8	30.9	30.5	29.3	.343	.100
27	.557	34.2	28.1	25.9	29.3	.314	.045
28	.525	38.5	30.8	27.2	29.3	.342	.065
29B	.462	40.1	28.4	23.4	30.5	.318	.035
Sub-Angular Sand							
25	.640	37.6	33.0	31.0	33.4	.364	.065
22	.619	37.8	32.8	30.4	33.4	.362	.055
23A	.586	39.6	28.8	28.0	32.0	.322	.050
24A	.562	42.4	32.8	27.5	32.5	.362	.040
Very-Angular Sand							
30	.969	35.6	32.5	31.0	33.5	.359	.090
31	.974	36.6	34.8	34.0	34.2	.381	.110
32	.814	40.6	32.6	28.2	33.5	.359	.060
33	.764	41.0	32.7	28.0	33.2	.361	.050

TABLE III DIRECT SHEAR TESTS ON SAND TYPE A-W HELD CONSTANT

TEST #	e_o	W(Kg)	ϕ°	ϕ_f°	ϕ_n°	ϕ_R°	μ	Δm(INCH)
				DRY TESTS				
Sub-Angular Sand								
50	0.672	24	35.3	29.1	26.7	34.7	.369	.045
51	0.672	12	37.8	32.3	29.7	35.2	.411	.045

TABLE IV DIRECT SHEAR TESTS ON SAND TYPE B - W VARIED

TEST #	e_o	$\bar{\sigma}_3$ (Kg/cm^2)	$\bar{\sigma}_1 - \bar{\sigma}_3$ (Kg/cm^2)	ϕ°
Round Sand				
1	.553	.960	2.21	32.3
3	.570	.960	2.10	31.4
5	1.350	.960	1.74	28.4
Sub-Angular Sand				
7	.706	.960	2.80	36.2
Very-Angular Sand				
2	.848	.925	3.26	39.6
4	.870	.960	3.10	38.1
6	1.00	.960	2.42	33.8

TABLE V DRY TRIAXIAL TESTS

SAND TYPE A

W(Kg)	p (gms/grain)
8	.301 gms
12	.452
16	.603
20	.753
24	.904
28	1.052
32	1.200

TABLE VI CALCULATED LOAD PER PARTICLE-DIRECT SHEAR TEST

BIBLIOGRAPHY

1. Terzaghi, K. Erdbaumechanik auf Bodenphysikalischen Grundlage, p. 399, 1925.

2. Mogami, T. "On the Law of Friction In Sand," Proc. 2nd Int. Conf. on Soil Mech. and Found. Eng. Vol. 1, p. 51, 1948.

3. Rowe, P. W. "A Stress-Strain Theory for Cohesionless Soil with Applications to Earth Pressures at Rest and Moving Walls," Geotechnique, Vol. 4, pp. 70-88, 1954.

4. Reynolds, O. "Experiments Showing Dilatancy, a Property of Granular Material, Possibly Connected with Gravitation," Scientific Papers by O. Reynolds, Vol. 2, pp. 217-227, 1886.

5. Taylor, D. W. Fundamentals of Soil Mechanics, John Wiley and Sons, Inc., pp. 345-351, 1948.

6. Hafiz, M. A. A. "Strength Characteristics of Sands and Gravels," A Thesis presented for the Degree of Doctor of Philosophy, University of London, 1950.

7. Bishop, A. W. Appendix , Thesis by M. A. A. Hafiz, see reference #6.

8. Newland, P. L. and Allely, B. H. "Volume Changes In Drained Triaxial Tests on Granular Materials," Geotechnique, Vol. 7, p. 17, 1957.

9. Bowden, F. P. "Adhesion and Friction," Endeavor, Vol. 16, pp. 5-18, 1957.

10. Bowden, F. P., and Young, J. E. "Friction of Diamond Graphite, and Carbon, and the Influence of Surface Films," Proc. Royal Soc. of London, Vol. 288, p. 244, 1951.

11. Tschebotarioff, G. P. Soil Mechanics, Foundations, and Earth Structures, McGraw-Hill, Inc., pp. 120-126, 1951.

12. Penman, A. D. M. "Shear Characteristics of a Saturated Silt, Measured in Triaxial Compression," Geotechnique, Vol. 3, pp. 312-328, 1952-3.

13. Norwegian Geotechnical Institute, Literature Concerning Friction In Sand--The Friction of Minerals, An Internal Report, F. 152, 1959.

14. Bjerrum, L., Kringstand, S., and Kummeneje, O. The Shear Strength of A Fine Loose Sand, Norwegian Geotechnical Institute, F. 9, 1958.

15. Wadell, H. "Sphericity and Roundness of Rock Particles," Jour. Geology, Vol. 41, p. 310, 1933.

16. Kolbuszewski, J. J. "General Investigation of the Fundamental Factors Controlling Loose Packing of Sands," Proc. 2nd Int. Conf. on Soil Mech. and Found. Eng. Vol. 7, pp. 47-49, 1948.

17. Hill, R. The Mathematical Theory of Plasticity, Oxford at the Clarendum Press, pp. 294-296, 1950.

18. Hertz, H. Theory of Elasticity, by Timoshenko, McGraw-Hill Book Co., Inc., p. 343, 1934.

19. Birch, F., Handbook of Physical Constants, Geological Society of America, paper #36, p. 45, 1942.